Evaluating a conceptual hydrological model at gauged and ungauged basins using machine learning-based limits-of-acceptability and hydrological signatures

Abhinav Gupta[1*], Mohamed M. Hantush[2], Rao S. Govindaraju[3]

[1]Department of Chemical and Environmental Engineering, University of Cincinnati

[2]Center for Environmental Solutions & Emergency Response, United States Environmental Protection Agency

[3]Lyles School of Civil Engineering, Purdue University

Correspondence to: Abhinav Gupta (gupta4ab@ucmail.uc.edu)

2660 Clifton Ave, Cincinnati, OH, 45221

This preprint has not been peer-reviewed.

Abstract. Hydrological models are evaluated by comparisons with observed hydrological quantities such as streamflow. A model evaluation procedure should account for dominantly epistemic errors in measured hydrological data such as observed precipitation and streamflow and avoid type-2 errors (rejecting a good model). This study uses quantile random forest (QRF) to develop limits-of-acceptability (LoA) over streamflow that accounts for the measurement uncertainties. A significant advantage of this method is that it can be used to evaluate models even at ungauged basins. In this study, this method was used to evaluate a hydrological model – namely the Sacramento Soil Moisture Accounting (SAC-SMA) in St. Joseph River Watershed (SJRW) – in gauged and hypothetical ungauged scenarios. Using LoA alone to account for uncertainty in data yielded a large number of models as behavioral, suggesting the need for additional measures to develop a more discriminating inference procedure. Five streamflow-based signatures (i.e., autocorrelation function, Hurst exponent, baseflow index, flow duration curve, and long-term runoff coefficient) were used to further eliminate physically unrealistic models which were considered behavioral by LoAs. The combination of LoAs over streamflow and streamflow-based signatures helped constrain the set of behavioral models in both gauged and ungauged scenarios. Among the signatures used in this study, Hurst exponent and baseflow index were the most useful ones. The NSEs of behavioral models ranged from 0 to 0.65. Very wide predictive uncertainty bounds were obtained in the ungauged scenario. Many of the behavioral models resulted in underestimation (overestimation) of observed high (low) flow. Overall, the methodology used in this study showed promise as a model inference strategy.

Keywords: Streamflow**,** Model (in)validation, Limits-of-acceptability, Machine learning, Prediction at ungauged basins

1. Introduction

Environmental models need to be evaluated against field observations for their fitness-of-purpose and their ability to model system dynamics (Hrachowitz et al., 2014; Beven, 2019; Parker, 2020). Hydrological models utilize precipitation data and other meteorological inputs to simulate fluxes such as streamflows and states such as soil moisture as outputs. For a model to be considered good, simulated hydrological quantities should be consistent with available corresponding observations. The model evaluation problem is complicated by the uncertainty due to presence of measurement errors in observed input and output quantities (e.g., Renard et al, 2010; Le Coz et al., 2014; Beven, 2019, 2023; Bardossy and Anwar, 2023). In what follows, the term 'model' will be used to refer to both model structures and any parameter set of a model structure.

Often, a single parameter set of a model structure that optimizes a goodness-of-fit (GoF) measure is used as the optimal parameter set (e.g., Knoben et al., 2019; Kratzert et al., 2019; Mai, 2023). In some cases, several optimal parameter sets, referred to as pareto optimal, are identified (Harvey et al., 2023). However, the idea of optimal parameter set is not well defined for hydrological models (Beven and Binley, 1992) because there often exist several parameter sets and model structures - referred to as equifinal models - that simulate the observed hydrological quantities approximately equally well over the period of available data (Beven, 2006). A single optimal parameter set obtained by a global optimization routine (e.g., Duan et al., 1992; Tolson and Shoemaker, 2007) depends upon the objective function being considered and the calibration period (Beven, 2023), and hence is ill-defined given a finite calibration period and a small number of observed hydrological quantities – in most studies only observed streamflow data are available to evaluate a model. Even though equifinal models may yield equally good streamflow estimates over the calibration period, their performance for other periods might be very different. A validation period is typically used for independent assessment of model performance, but different parameter sets may perform equally well for a validation period also. Also, equifinal parameter sets may yield very different simulations of internal fluxes and states (Gallart et al., 2007; Khatami et al., 2019; Hughes and Farinosi, 2021). Equifinality may also exist in terms of model setup pre-calibration such as discretization (Refsgaard et al., 2022).

Many methods have been proposed within the hydrologic literature to evaluate models and quantify uncertainties (see Gupta and Govindaraju (2022) for a recent review) including formal Bayesian methods (e.g., Kuczera et al., 2006), frequentist methods (Pande 2013a, 2013b), information-theoretic methods (Gong et al., 2013; Weijs et al., 2010a; 2010b; 2013), and generalized likelihood uncertainty estimation method (GLUE; Beven and Binley, 1992). The formal statistical methods use a probabilistic likelihood function to quantify the information in hydrological data and are based on aleatoric assumptions about the uncertainties. Thus, these methods are not applicable in hydrological modeling without strong assumptions because uncertainties encountered in hydrology are dominantly epistemic (Beven, 2019). Epistemic uncertainties by definition are the uncertainties of which statistical properties are unknowable for a given amount of data (Gupta and Govindaraju, 2022). These errors may vary from event to event in an arbitrary but non-random manner and are nonstationary (Beven, 2016; Gupta and Mackenna, 2023, preprint). Further, there can be observed events that do not satisfy mass balance or other physical constraints and are referred to as disinformative periods (Beven and Westerberg, 2011). These disinformative periods may introduce biases during parameter estimation and affect the antecedent conditions for subsequent events (Beven and Smith, 2015). Therefore, it is very difficult to realistically define probabilities in the case of epistemic errors (Berger and Smith, 2018) even though probabilities have a sound epistemic underpinning (Jaynes, 2002; Montanari, & Koutsoyiannis, 2012). To some extent, the problem of wrong assumptions can be addressed by making inference in spectral space, but this method has limitations as well (Schaefli and Kavetski, 2017; Gupta and Govindaraju, 2022). Moreover, Information-theory based GoF metrics do not treat the uncertainties explicitly and are often used for finding an optimal parameter set.

The idea of multi-objective optimization has also been used in hydrological modeling (e.g., Yapo et al., 1998; Efstratiadis, & Koutsoyiannis, 2010; Shafii et al., 2015; Harvey et al., 2023) where several models are obtained by optimizing multiple objectives simultaneously. These studies show that no single model is best for all the objective functions. A set of models, referred to as Pareto front, is obtained such that no model in the set is better or worse than other models in terms of all the objectives. While Pareto fronts address some of the problems with identifying a single model based on a single objective function, they do not address issues arising from uncertainty in the data and several good models might be rejected (type-2 error) in the process.

In the GLUE framework, non-probabilistic likelihoods, also referred to as informal likelihoods, are used to assess the information content in hydrological data. The informal likelihood may be any GoF metric such as Nash-Sutcliffe efficiency (NSE). The idea behind using informal measures is that they reduce the over-conditioning of the parameter sets on data (e.g., Smith et al., 2008). The main limitation of the early application of informal likelihood measures was that the modeler had to decide the threshold value of NSE (or any other GoF metric) beyond which a model could be deemed behavioral. This is a difficult choice to make given the uncertainties in hydrological data and introduces subjectivity. Also, GoF measures collapse all the information in hydrological data into a single number, and thus, may not be able to represent information in hydrological data well (Gupta et al., 2008). However, several such GoF measures emphasizing different parts of the hydrograph (or another response variable) may be used in combination to address this problem, as is done in multi-objective optimization, but the fundamental problem remains that these measures do not explicitly account for uncertainties.

The limits-of-acceptability (LoA) method has been proposed within the GLUE framework to address some of the limitations of early GLUE applications (Beven, 2006; Liu et al., 2009; Krueger et al., 2010; Coxon et al., 2014; Hollaway et al., 2018; Beven, 2019; Beven and Lane, 2022). LoAs should be defined as the upper and lower bounds over streamflow (or any other relevant quantity) such that these bounds reflect the effects of errors in hydrological data (Beven et al., 2022; Gupta et al., 2023a). Thus, a model that simulates streamflows within LoAs (while accounting for potential outliers) may be considered as being consistent with the data. The goal is to identify all the models that simulate streamflow within LoAs. Note that this approach is different from identifying the good models based on comparing observed and simulated streamflow. Further, LoAs must be defined before any model calibration to avoid interactions between measurement and structural uncertainties. Several attempts have been made to model rainfall, streamflow and structural errors separately (e.g., Renard et al., 2010), however these studies show that the parameters of these models cannot be identified without strong prior information on these errors. Further, since LoAs are defined for each time step; a model can be evaluated at the timestep level using the LoA framework.

The main advantage of the LoA method is that the conditions of model acceptability are defined before any model evaluation takes place. Once the LoAs are defined, a likelihood function can be based on the LoAs, which can then be used either in the GLUE framework or formal Bayesian framework (Nott et al., 2012). Even a Gaussian distribution, which forms the basis of many formal Bayesian studies, can be used to define a likelihood function by truncating it at LoAs, even though informal options may be more suitable depending on the application. The traditional applications of formal Bayesian methods do not impose any limits on the spread of the Gaussian distribution, allowing a greater interaction between structural and measurement uncertainties. Indeed, the formal Bayesian methods assign a small probability to bad models but do not reject them (Lindley, 2006), while GLUE and LoA methods follow a rejectionist framework.

Often, LoAs are defined based on streamflow uncertainty only, and the effect of precipitation uncertainty is included by subjectively increasing the width of the LoA (e.g., Krueger et al., 2010; Coxon et al., 2014). In some studies where LoAs were based only on streamflow uncertainty (e.g., Hollaway et al., 2018), all the evaluated models were rejected. Beven (2019) proposed a method to define LoAs based on variability of runoff ratios of rainfall-runoff events. This method accounts for both the precipitation and streamflow measurement uncertainties, but the method is applicable to flashy watersheds only and cannot account for timing errors.

Gupta et al. (2023a) proposed a decision tree (DT) based method to define LoAs. This method accounts for the effects of both streamflow and precipitation uncertainty. One of the advantages of the DT method is that it can use data from *donor watersheds* (watersheds other than the watershed where the model is to be evaluated) to define LoAs. Hence, DTs can be used to define LoAs for both gauged and ungauged catchments. Gupta et al. (2023a) derived DT-based LoAs for four subbasins located within St. Joseph River Watershed (SJRW). This study builds on Gupta et al. (2023a) by applying these LoAs to evaluate a hydrological model.

One interesting application of DT-based LoA is that it can be used to evaluate a hydrological model even at ungauged locations. Prediction at ungauged basins (PUB) is one of the most important and challenging problems in hydrological science (Hrachowitz et al., 2013). To constrain the simulations in an ungauged basin, information is transferred from similar donor watersheds to the parent watershed by parameter regionalization or streamflow signature regionalization (Razavi and

Coulibaly, 2013). Essentially, rainfall-runoff process in the ungauged watershed is inferred using the data from other similar gauged catchments. But the regionalization process has significant additional uncertainty which is also difficult to quantify (Wagener and Montanari, 2011). DT-based LoAs can be useful for addressing the PUB challenge by providing a simple metric to evaluate models at ungauged locations while accounting for data uncertainties. Also, DT-LoAs allow model evaluation at each time-step as opposed to integrated measures of model evaluation measure provided by signature-based constraints. Therefore, this study also explores the suitability of ML-based LoAs in evaluating models.

If the uncertainties in data are large, several models might be consistent with the observed streamflow time series, but many of these models may not necessarily represent catchment dynamics satisfactorily (Hrachowitz et al., 2014). To address this problem, the use of hydrological signatures has been proposed (Gupta et al., 2008; Euser et al., 2013; Hrachowitz et al., 2014; Fenicia et al., 2018; Kavetski et al., 2018). According to this methodology, a model can only be accepted as behavioral if it reproduces the observed signatures, along with observed sequences of streamflow. An example of such a signature-based constraint is the long-term runoff coefficient (LRC) of a watershed (Kiraz et al., 2023); the simulated LRC should equal the observed LRC within the margin of errors. It is believed that the effect of errors in precipitation and streamflow will be reduced over a long timescale because of cancellation of errors (e.g., Kavetski et al., 2018; Gupta and Mackenna, 2023, preprint). These constraints can be referred to as soft constraints. In this study, the role of signature-based soft constraints in identifying behavioral models will also be explored. The use of soft constraints can be particularly beneficial in ungauged catchments (e.g., Dal Molin et al., 2023).

The objectives of the study were as follows:

(1) To test the suitability of DT-based LoAs for evaluating a conceptual hydrological model,

(2) To understand the impact of input and streamflow uncertainties on hydrological model evaluation,

(3) To evaluate the capability of streamflow-based signatures (soft constraints) in identifying nonbehavioral models,

(4) To explain why a model is rejected or accepted as a behavioral model.

The main novelty of this paper lies in using DTs to evaluate a hydrological model. This method accounts for both precipitation and streamflow uncertainty; other methods (except the runoff-ratio method) neglect precipitation uncertainty. A significant advantage of DTs is that they can be used for regionalization of streamflow to evaluate a hydrological model at ungauged locations at time-step level, while accounting for uncertainties. Further, a well-known spectral property of streamflow time series called long-term persistence (discussed below) has been used as streamflow-based signature – this signature can be applied at both gauged and ungauged locations. To the best of authors' knowledge, this paper provides the first attempt to test the utility of long-term persistence as a signature for model evaluation at both gauged and ungauged locations (see Westerberg and McMillan, 2015; McMillan et al., 2021 for a review of signatures used in hydrology; also see Yadav et al., 2007; Shafii and Tolson, 2015). We note that other spectral properties such as auto-correlation function etc. have been used in earlier studies to calibrate hydrological models (Winsemius et al., 2009; Castiglioni et al., 2010; De Vleeschouwer and Pauwels, 2013), but long-term persistence seems not to have been used in this context. Typical hydrological modeling studies calibrate a model either in time domain or signature domain (e.g., Coxon et al., 2014). The 'signature domain only' calibration is done to avoid the biases introduced by systematic errors in hydrological data (Fenicia et al., 2018), but signatures may lose some of the information contained in streamflow time series. Thus, this study combines calibration in time domain and signature domain. Using LoAs over streamflows only may result in acceptance of physically unrealistic simulations; signatures are used to identify these unrealistic simulations.

2. Hydrological model and data

2.1 Hydrological Model

The Sacramento Soil Moisture Accounting (SAC-SMA; Burnash, 1995) model along with a snow model and runoff routing model was used in this study. SAC-SMA has been used in several studies to simulate streamflow (Sorooshian et al., 1993; Vrugt et al., 2006; Kratzert et al., 2019). It is a conceptual model with several parameters requiring calibration. Two other models, a snow model and a runoff routing model, were used along with SAC-SMA. The SAC-SMA model simulates infiltration, percolation, evapotranspiration, and surface runoff. The runoff routing model routes the runoff to a streamflow outlet. Evapotranspiration calculations were based on potential evapotranspiration, calculated using the Hamon equation (Hamon, 1963). The snow model used was snow-17 (Anderson, 1976), and the routing model used was unit hydrograph represented by gamma distribution. The combined model has a total of 24 parameters that were varied within predefined ranges to simulate streamflow and other hydrological fluxes. A list of these parameters along with their ranges, as used in this study, is provided in Table 1.

2.2 Study area

Four subwatersheds in St. Joseph River Watershed (SJRW) were used as test cases in this study (Fig. 1). SJRW drains a total area of approximately 3000 km^2, overlapping the states of Michigan, Indiana, and Ohio in eastern USA. Climate in this watershed is characterized by hot summers and cold winters, with precipitation falling throughout the year. Snowfall is an important component of the hydrological cycle. Major land use type is cropland and forest (Mallya et al., 2020). The four SJRW stations are identified by their USGS (United States Geological Survey) station number at the outlet where streamflows are measured. A list of these stations along with some of the characteristics of corresponding drainage areas are provided in Table 2.

2.3 Hydrological data

Data from six NCDC (National Climate Data Center) rain gauges outside but near the SJRW were used to compute daily areal average precipitation using the Thiessen polygon method. Other meteorological data required for the SAC-SMA are average daily temperatures which were also available from the six NCDC stations. Mean daily streamflow data were available from the USGS website. Data from calendar years 2001-2016 were used in this study, with 2001-2010 data being used for identifying behavioral models and the remaining data being used for independent validation. For three of the gauges (04180500, 04180000, 04178000) the year 2001 was used as the warm-up period and the years 2002-2010 were used for model evaluation (or calibration). For the gauge 04179520, year 2002 was used as the warm-up period and the years 2003-2010 were used for model evaluation, because data for the year 2001 were not available for this station.

In addition, data from 431 watersheds located in Ohio River Basin (ORB) were used to develop a machine learning (ML) model. Some details of these watersheds can be found in Gupta et al., (2023a). Data from ORB were used to regionalize streamflow in ungauged scenario and to augment the training data in gauged scenario (explained below).

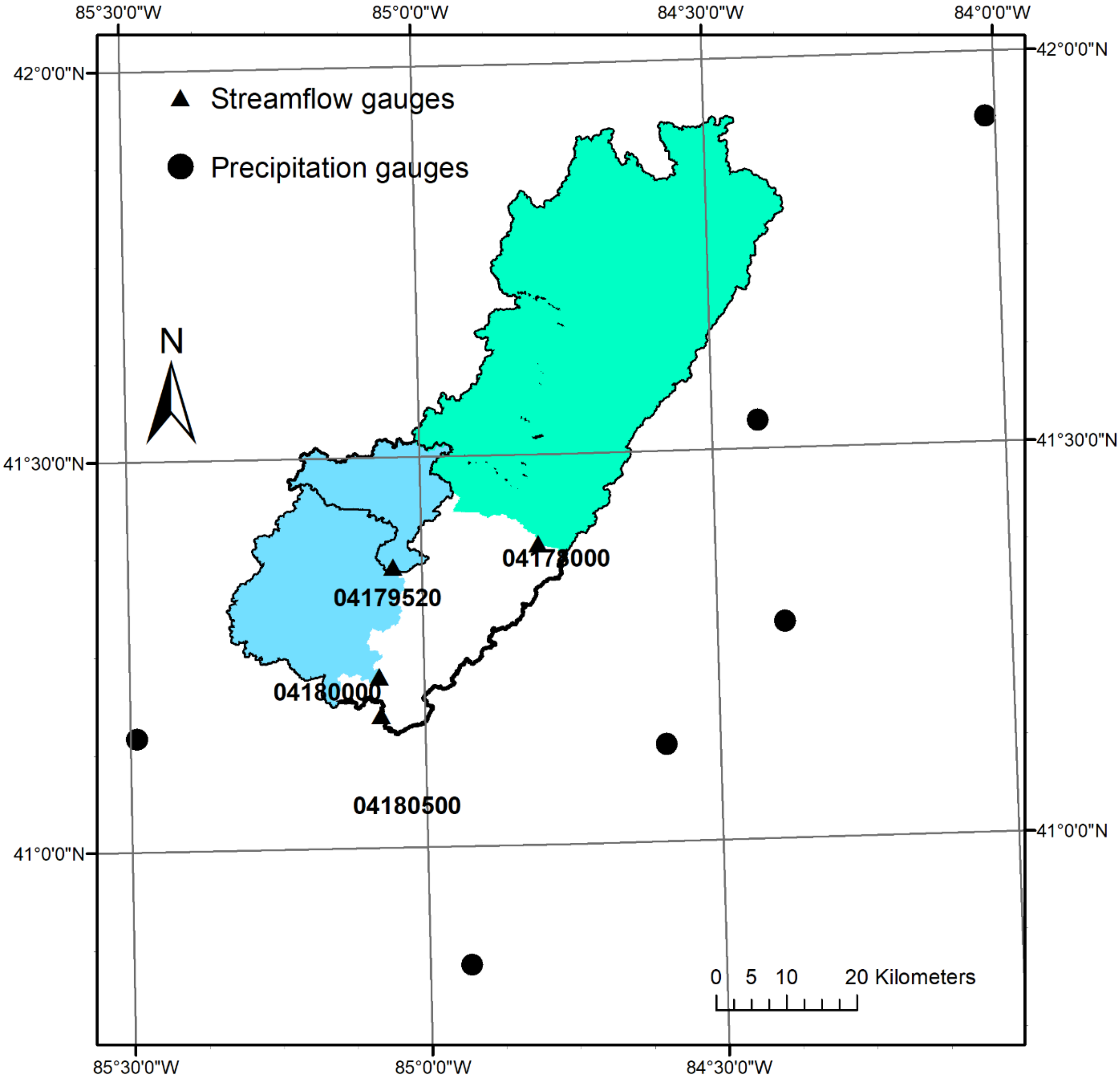

Figure 1. St. Joseph River Watershed (SJRW) with drainage areas of the four USGS stations and rainfall gauges

Table 1. Parameters of the hydrological model along with their initial range

	Parameter	Range
Snow parameter	SCF	[0.1, 5]
	PXTEMP	[-1, 3]
	TTI	[0, 0]
	MFMAX	[0.80, 3]
	MFMIN	[0.010, 0.79]
	UADJ	[0.010, 0.40]
	MBASE*	0
	TIPM	[0.01, 1]
	PLWHC	[0.01, 0.40]
	NMF	[0.040, 0.40]
	DAYGM	[0.010, 0.50]
Hydrological parameter	UZTWM	[1, 800]
	UFWM	[1, 800]
	LZTWM	[1, 800]
	LZFPM	[1, 1000]
	LZFSM	[1, 1000]
	UZK	[0.10, 0.70]
	LZPK	(0, 0.025]
	LZSK	(0, 0.25)
	ZPERC	[1. 250]
	REXP	[0, 6]
	PFREE	[0, 1]
	PCTIM*	0
	ADIMP*	0
	RIVA*	0
	SIDE*	0
	RSERV	[0, 1]
Routing parameters	Shape parameter (α)	[1, 5]
(Unit hydrograph: $\frac{1}{\beta^{\alpha}}\Gamma(\alpha)x^{\alpha-1}\,exp\left(-\frac{x}{\beta}\right)$)	Scale parameter (β) (days)	(0, 150]
Evapotranspiration parameter	Hamon model parameter	[1.26, 1.74]

*Parameters that were not calibrated

Table 2. List of St. Joseph River Watershed (SJRW) stations. The method to estimate baseflow ranges has been described in the Appendix A. The values of BFI, LRC and H are based on calibration period data.

USGS station	Drainage Area (km^2)	Elevation (m)	Baseflow index (BFI) range	Long-term Runoff Coefficient (LRC)	Hurst exponent (H)
04180500	2745.40	281.58	0.25 – 0.54	0.375	0.72
04180000	699.30	277.02	0.26 – 0.58	0.387	0.76
04179520	233.62	286.53	0.30 – 0.59	0.377	0.86
04178000	1579.90	291.4	0.34 – 0.76	0.386	0.78

3. Model evaluation

3.1 Limits-of-Acceptability and likelihood function

The details of LoA construction using DTs can be found in Gupta et al. (2023a). Briefly, a DT-based method called quantile random forest (QRF) was used to define LoA. QRF is a tree-based ML model that yields a distribution for the response variable for a given predictor vector. In QRF, the predictor space is divided into several contiguous and non-overlapping sub-regions. This division is carried out using the calibration/training data; the algorithm for defining these sub-regions can be found in any ML textbook (e.g., Hastie et al., 2001). To determine the distribution of the response variable for any predictor vector, first the sub-region to which the predictor vector belongs is determined and then the training samples falling in each sub-region are used to define the distribution. The process of division of predictor space into several sub-regions can be visualized as a tree (see Fig. 2 in Gupta et al., 2023a). Division of predictor space is carried out iteratively which can be visualized as growth of the tree into different nodes. The nodes obtained after the final iteration are referred to as leaf nodes.

In this study, QRF models were developed using the predictor variables listed in Table 3 and streamflow was the response variable. Therefore, QRF yielded a distribution of streamflow values for a given predictor vector. This distribution represents all the possible streamflow values while accounting for errors in hydrological data. A similar argument to define LoAs was also made in Winsemius et al. (2009); these authors defined LoAs over some streamflow signatures based on interannual variability of the signatures. Gupta et al. (2023a) claimed that LoAs defined using QRF can account for both precipitation and streamflow uncertainty because QRF groups similar predictor variables (predictor vectors that are close to each other in predictor space) into leaf nodes and the large difference between responses can be attributed either to lack of relevant predictor variables and errors in predictor variables (primarily precipitation and temperature in this study) and response variables (streamflow in this study).

When constructing LoAs using QRF, one has to decide the lower and upper percentiles of response variable in a leaf node to be used as lower and upper LoAs. In what follows, the results corresponding to 1st percentile and 99.5th percentiles will be discussed in detail. The 97.5th percentiles were also used to define upper LoAs; these results are presented in Supplementary Information (SI) and only sparingly discussed in the main text.

In this study, three QRF models were used to test the applicability of LoA concept in three different scenarios:

(1) Gauged-single scenario (LoA_{GS}): The QRF models were trained using data from only the watersheds where the LoAs were to be constructed. For example, to construct LoAs for the station 04180500, data from only this station were used. In this case, the meteorological data were used as inputs and streamflow as output.

(2) Gauged scenario (LoA_G): The QRF models were trained using data from multiple watersheds including data from the station where LoA were to be constructed. In this study, data from 431 watersheds in Ohio River Basin (ORB) along with the data from the four SJRW stations were used to develop this model (see Gupta et al., 2023 for details).

(3) Ungauged scenario (LoA_{UG}): The QRF model was trained using data from only the ORB watersheds; data from the four SJRW stations were not used to train the model. This scenario represents the ungauged case when data are not available at the station where a hydrological model is to be evaluated.

The gauge-single scenario represents the case where we focus on data from a single watershed to develop a hydrological model. The gauged scenario represents the case where data from several watershed are available and are used here to test the utility of such a dataset in terms of model validation in a particular watershed – this has become a popular practice in ML application for streamflow prediction (e.g., Kratzert et al., 2019). The ungauged scenario is used to test the usefulness of data across multiple watersheds in terms of model evaluation in a particular watershed where streamflow data are not available. The LoAs were constructed using data from the calibration period (2001-2010) and the remaining data (2011-2016) were kept as an independent validation period.

In ungauged scenario, QRF model was trained using data from 431 ORB watersheds and data from SJRW stations were not used. Therefore, we expect that the transfer of information from gauged to ungauged location would incur additional uncertainty. Gupta et al. (2023a) tested the developed models in terms of their ability to simulate observed streamflow. The tests were carried out in the ungauged scenario as it is a more stringent test. The NSE values obtained for the stations 04180500, 04180000, 04179520, and 04178000 were 0.57, 0.63, 0.60, and 0.36, respectively.

These NSEs seem good enough to define LoAs except for the station 04178000 (Gupta et al., 2023a). But LoAs developed even for the station 04178000 were quite useful. Gupta et al. (2023a) further showed that LoAs constructed for these four stations accounted for the effects of streamflow and precipitation measurement uncertainty. Effect of random streamflow uncertainty were approximated using the probabilistic rating curve analysis. Effects of potential epistemic uncertainties in peak streamflow values was also tested: it was shown that LoAs obtained would envelop the true peak streamflow values even if the observed values were underestimates of true values by up to 100%. The typical errors in peak streamflow have been reported to be 20–40% (Di Baldassarre and Montanari, 2009). The uncertainty in precipitation was estimated using the Monte-Carlo sampling of the rain-gauges without replacement. Further, the LoAs obtained using the QRF method were compared against those obtained by using the runoff-ratio method. Some other properties of the LoAs obtained using the QRF method are discussed below.

Table 3. Predictor variables in machine learning models to estimate streamflow time series at a station in a river-network. Exploratory statistics in the third column represent (minimum, maximum, median, and mean). (From Gupta et al., 2023a)

Predictor variable	**Description**	**Exploratory Statistics**
Drainage area (Km^2)	Cumulative drainage area of streamflow station	(7.74, 250260, 624, 4187)
Impervious Area*(%)	Percentage of impervious area	(1.92, 7.74, 6.36, 6.44)
Sand content**(%)	Percentage of sand content	(6.34, 49.61, 20.97, 19.78)
Clay content (%)	Percentage of clay content	(15.88, 45.12, 26.03, 27.58)
Conductivity ($\mu m\ s^{-1}$)	Average hydraulic conductivity of the drainage area	(0.01, 77.22, 0.19, 3.51)
Permeability ($cm\ hr^{-1}$)	Average permeability of the drainage area	(1.02, 15.09, 3.87, 4.82)
Rainfall***	Total daily rainfall during current and previous 1, 7, and 30 days	–
Snowfall	Total Daily snowfall during current and previous 1 and 30 days	–
Snow depth	Daily snow depth during current and previous 1 and 30 days	–
Temperature	Average daily maximum and minimum temperature at current day	–

* Land-use data were collected from NLCD database

** Soil data were collected from STATSGO database

*** Climate data were collected from Global Historical Climatology Network (GHCN) database

Streamflow time series were simulated using a total of 10^6 parameter sets sampled uniformly from the parameter space (Table 1). A parameter set was considered behavioral if it satisfied the following four criteria:

(1) At least $(1-\alpha)100\%$ of the simulated streamflows are enveloped by the LoA.

(2) At least $(1-\alpha)100\%$ of the simulated rising limb flows are enveloped by the LoA.

(3) At least $(1-\alpha)100\%$ of the simulated recession flow are enveloped by the LoA.

(4) At least $(1-\alpha)100\%$ of the peak streamflow values, identified as greater than 90 percentile streamflow value, are enveloped by the LoA.

These criteria were used to ensure that all parts of the hydrograph are well simulated by a behavioral parameter set. Otherwise, it is possible that a parameter set simulates the high streamflow within LoAs but does not simulate the low flows well at several timesteps. These criteria maybe varied depending upon the intended application of the model. Two values of α were used: $\alpha = 0.05$ (5% outliers) and $\alpha = 0.00$ (no outliers). The $\alpha = 0.05$ is used to allow for outliers since LoAs are defined using only 10 years of data, leaving room to accommodate future surprises. When $\alpha = 0.00$, a parameter set was considered behavioral only if it simulated streamflow within LoA at all the time steps (no outliers).

Each behavioral model was assigned a likelihood value using the following procedure. First, each time-step in the calibration period was assigned a score between -1 to 1 using the equation (Hollaway et al., 2018)

$$Score_t = \begin{cases} (\hat{y}_t - y_t)/(LU_t - y_t), & (\hat{y}_t - y_t) \geq 0 \\ (\hat{y}_t - y_t)/(y_t - LL_t), & (\hat{y}_t - y_t) < 0 \end{cases} \tag{1}$$

where $Score_t$ denotes the score value at timestep t, $\hat{y}_t$ denotes simulated value at timestep t, y_t denotes observed value at timestep t, LU_t and LL_t denote the upper and lower LoAs at timestep t, respectively. A positive (negative) score value at a time step implies overprediction (underprediction). Second, each timestep was assigned a weight based on their score as follows:

$$W_t = \begin{cases} 1 - Score_t, & 0 \leq Score_t \leq 1 \\ (1 + Score_t)^2, & -1 \leq Score_t < 0 \\ 0, & \text{othewise} \end{cases} \tag{2}$$

Finally, the likelihood $L(M)$ of a model M was computed as follows:

$$L(M) = C\left[\frac{1}{T}\sum_{t=1}^{T}\frac{|y_t - \hat{y}_t|}{(W_t + \delta)}\right]^{-1}, \tag{3}$$

$$\delta = \min\{W_t | t \in [1, T], W_t \neq 0\},$$

where T denotes the number of calibration timesteps and C is the scaling factor so that likelihood values for different models sum up to one. Underpredictions were penalized more heavily in the computations of weights (Eq. 2) because QRF defines LoAs such that models with underpredictions are more likely to be accepted than the ones with overpredictions as both observed and simulated streamflow are bounded below by zero and LL_t defined by QRF are close to zero; thus, LoAs are biased toward models underpredicting streamflow as behavioral. Further, this likelihood function was defined following the intuition that (1) the models that simulate streamflow with large deviations from the observed streamflow should get lower likelihood, and (2) the timesteps at which streamflow is simulated outside the defined LoAs should be penalized more heavily.

Predictive uncertainty at a timestep was computed as the 99% credible region defined using the 0.5th and 99.5th percentiles of simulated streamflows using behavioral parameter sets and for both calibration and validation periods. The percentile values were defined based on the cumulative distribution function (CDF) at each timestep which, in turn, could be obtained using the likelihood values as defined in Eq. (3).

3.2 Streamflow-based signatures

Five streamflow-based hydrological signatures were used to further constrain the acceptable model behaviors. These constraints include autocorrelation function (ACF) of streamflow time-series, Hurst exponent (H) of streamflow time series, baseflow index (BFI), flow duration curve (FDC), and long-term runoff coefficient (LRC). The observed and simulated signatures were compared to check whether the simulated signatures reflect the expected watershed function. These signatures are summarized in Table 4.

For a model to be accepted as behavioral by ACF constraint, the NSE between observed and simulated ACF for the lags 1-100 days should be greater than 0.6. For a model to be acceptable as behavioral by the FDC constraint, the NSE between observed and simulated FDCs should be greater than 0.6. The comparison between the two FDCs was done using the flow value at and between 5th and 95th exceedance probability equally spaced by 5 percentiles. For a model to be accepted as behavioral by the LRC constraint, the simulated LRCs should be between $0.6LRC_{obs}$ and $1.4LRC_{obs}$. Signature values may also be affected by data uncertainty (Westerberg and McMillan, 2015); therefore, the acceptance criteria on these signatures were set to wide margins to avoid false negative errors (rejecting a good model). For example, Westerberg and McMillan (2015) reported $\approx +20\%$ uncertainty in LRC with rain-gauge density of $\frac{1}{135}\,\mathrm{km}^{-2}$ for 135 km^2 Brue catchment.

To compute observed BFI, first baseflow was estimated using the method proposed by Collischonn and Fan (2013) and then, BFI was computed as the ratio of total baseflow and total streamflow. Simulated baseflow was obtained directly from the SAC-SMA as one of the outputs. In this study, the method of Collischonn and Fan (2013) was used to compute a range of BFI values instead of just one BFI value (Appendix A). According to the BFI constraint, a model was accepted as behavioral only if it simulated BFI within this range (see Table 2 for the range of BFI values used for different test watersheds).

Hurst exponent of a simulated streamflow time series was estimated using the periodogram of the time series. Periodogram of a time series is very noisy irrespective of the amount of data available to estimate it (Priestley, 1982); therefore, a piecewise linear curve was fitted to the estimated periodogram (Kim et al., 2015). The streamflow periodogram can be approximated by $|\omega|^{1-2H}$ as ω approaches zero (Beran, 1994), where H denotes the Hurst exponent and ω denotes the frequency in radians/day. Thus, H was estimated by

$$H = -\frac{s}{2} + 0.5, \tag{4}$$

where s denotes the slope of the periodogram on log-log plot near $\omega = 0$.

There are several methods to estimate H (see Montanari et al., 1999) but these methods yield significantly different value of H. Perhaps the best method to estimate H value is to fit a stochastic FARIMA model to streamflow time series (Montanari et al., 1997; Gupta et al., 2023b); but this method is computationally infeasible for this study as it takes significant computational resources for just one streamflow time series, making it practically impossible to implement for 10^6 simulated time series. Equation (4) was adopted in this study. It is known that the H value for a typical streamflow time series lies between 0.5 and 1 (Montanari et al., 1997; Mudelsee, 2007). Indeed, Gupta et al. (2023b) fitted FARIMA models to streamflow time series from more than 500 watersheds across the USA; all of the models were well fitted to the time series with H value between 0.5 to 1. Therefore, H value of a simulated streamflow time series should fall between 0.5 and 1 for a model to be accepted as behavioral according to this constraint. A relaxed limit has been used on H because of difficulties in estimating H values and to avoid rejecting good models. It will be shown that even this relaxed limit on H can be helpful in identifying non-behavioral simulations.

The periodogram of a stationary stochastic time series is the sample estimate of power spectral density which, in turn, is the square of the absolute values of the Fourier coefficients of the corresponding autocorrelation function (Priestley, 1982). Therefore, signature ACF and H used in this study are closely related to each other. However, the ACF signature cannot be used in ungauged scenario. But H can be used in both gauged and ungauged scenarios, since we constrain H value of simulated streamflow between 0.5 and 1.0, irrespective of the H value of the observed streamflow series. Similarly, none of the other signatures (FDC, BFI, and LRC) can be used in the ungauged scenario unless the value of these signatures is estimated using the data from donor watersheds which themselves have significant uncertainties associated with them (e.g., Dal Molin et al., 2023). Nevertheless, the simulations with extremely high or low values of BFI may still be rejected as non-behavioral in ungauged basins. In this study, simulations with BFI values of less than 0.10 or greater than 0.90 were considered non-behavioral in ungauged basins.

Table 4. Streamflow signatures. All the signatures were computed for the calibration period.

Signature	**Abbreviation**	**Applicability**	**Description**	**Acceptance criterion**
Autocorrelation function	ACF	Gauged	Autocorrelations of streamflow time series for the lags of 1 to 100 days	NSE between observed and simulated ACF should be greater than 0.60.
Hurst exponent	H	Gauged and ungauged	Hurst exponents of time-series obtained from the slope of the power spectral density (estimated by periodogram) of the streamflow time series	H should fall between 0.5 and 1.
Flow duration curve	FDC	Gauged	Values of FDC at and between 5 and 95% exceedance probabilities spaced by 5 percentiles	NSE between observed and simulated FDC should be greater than 0.60.
Baseflow Index	BFI	Gauged and ungauged	Ratio of total baseflow to the total streamflow over the entire calibration period excluding the baseflow period	Simulated BFI should fall between a minimum (BFI_{min}) and maximum (BFI_{max}) listed in Table 2. For ungauged scenario, BFI_{min} = 0.10 and BFI_{max} = 0.90
Long-term runoff coefficient	LRC	Gauged	Ratio of simulated to observed streamflow	Simulated LRC should be greater than 60% and smaller than 140% of observed LRC

4. Results

4.1 Limits-of-acceptability (LoAs) and number of behavioral models

Figure 2 shows the LoAs obtained by QRF method in the three scenarios along with observed streamflow and precipitation. Here, 99.5th percentiles were used to define upper LoAs. The LoAs obtained by using 97.5th percentile values are shown in Fig. S1 (SI). The three LoAs envelop the observations at most of the time-steps. This is also evident from Table 5 which lists the fractions of observations enveloped by the LoAs. The LoA_{UG} were the widest. The LoA_G and LoA_{GS} were similar at most of the timesteps except at the two major peaks. The wider LoAs obtained in ungauged scenario are desirable since we want to include as many rainfall-runoff behaviors as possible and we expect larger uncertainty in model simulations at ungauged basins. The lower LoAs were close to zero at all the timesteps because of using 1^{st} percentile in the leaf nodes as the lower LoAs. Models consistently underpredicting observed streamflow are less likely to be rejected even if they are bad simulators of a watershed's hydrological processes, thus needing to penalize underpredictions more heavily in the likelihood function (Eq. 2).

There were timing errors between observed peaks and LoA peaks (for example, at time step 2630); the timing errors were pronounced at gauge 04178000. These timing errors are likely due to timing errors in observed precipitation (Gupta et al., 2023). Notably, these timing errors were absent in LoA_{GS} in several cases and may be attributed to compensation of local epistemic errors in precipitation by gauged-single model. Another notable feature is presence of peaks in LoAs at some time steps where the streamflow is in recession phase - again likely due to potential epistemic uncertainty in precipitation. These features have been discussed in detail in Gupta et al. (2023a).

Table 6 lists the number of models accepted as behavioral for each scenario, for the two cases: (i) when 5% outliers were allowed and (ii) when no outliers were allowed. The number of behavioral models were very different when 99.5^{th} percentiles were used as upper LoAs compared to when 97.5^{th} percentiles were used as upper LoAs. The number of accepted behavioral models were significantly larger in the ungauged scenario which is expected given the wider LoAs in this scenario. Interestingly, when no outliers were allowed and 97.5^{th} percentiles were used as the upper LoA, no behavioral models were identified in the gauged scenario for any of the four watersheds. In other cases, the gauged scenario yielded larger number of behavioral models compared to those in gauged-single scenario for the watersheds 04180500 and 04180000; the gauged-single scenario yielded larger number of behavioral models for the other two watersheds. In summary, the number of behavioral models depends strongly on the way LoAs are constructed.

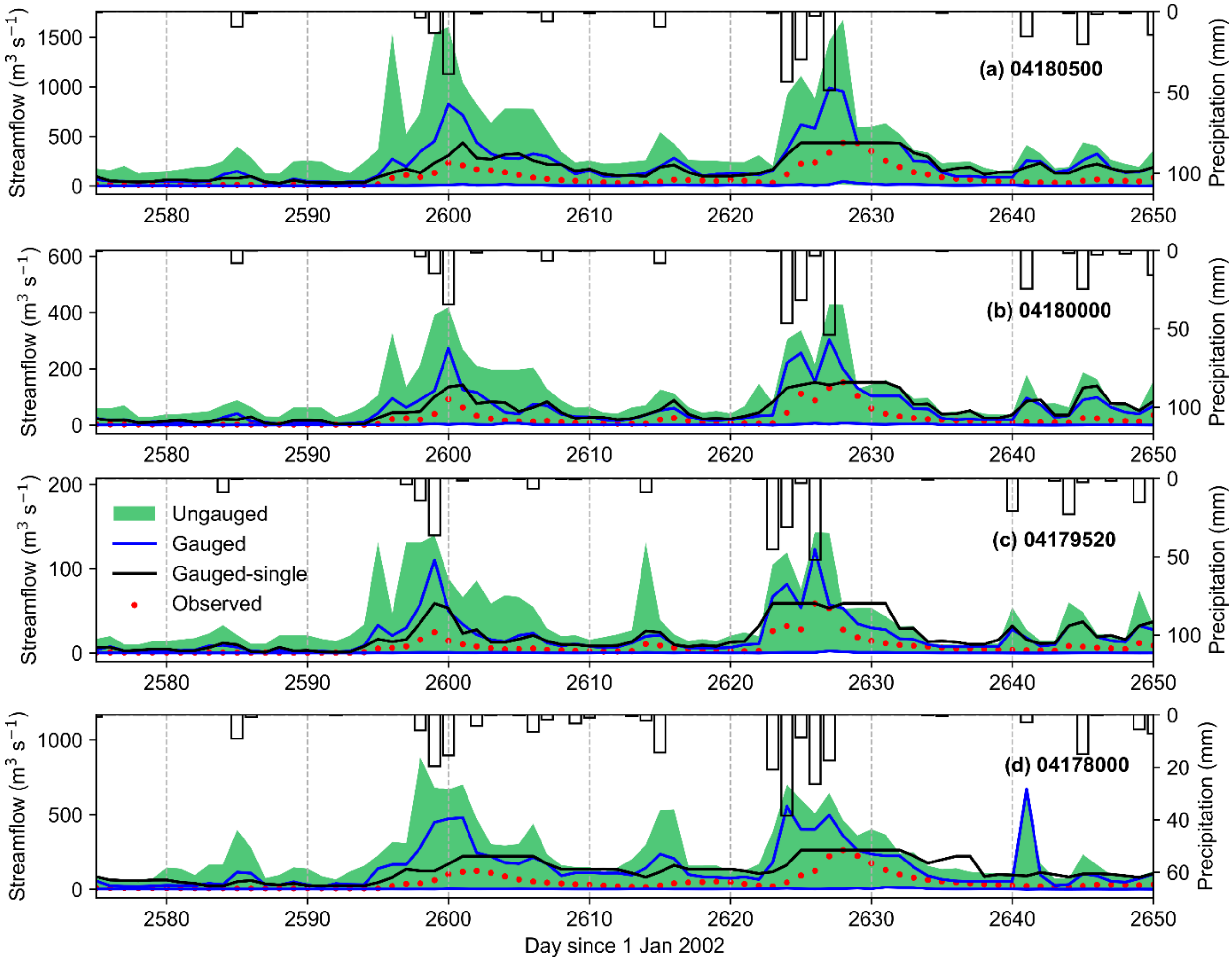

Figure 2. Using 99.5th percentile. Limits-of-acceptability (LoAs) obtained for the four watersheds in three scenarios: Ungauged (green band), Gauged (blue band), and Gauged-single (black band), along with observed streamflow (red dots) and precipitation. The upper LoA bounds were determined using 97.5th percentiles.

Table 5. Fractions of observations enveloped by the LoAs when the upper LoAs were defined by 97.5^{th} and 99.5^{th} percentiles. Lower LoAs were defined by using 1^{st} percentile in both the cases.

Gauge	Using 97.5^{th} percentile as upper LoAs			Using 99.5^{th} percentile as upper LoAs		
	Ungauged	Gauged	Gauged-single	Ungauged	Gauged	Gauged-single
04180500	0.992	0.997	0.999	0.998	0.999	0.999
04180000	0.994	0.995	0.997	0.999	1.000	0.998
04197520	0.995	0.991	0.997	0.999	0.999	0.997
04178000	0.987	0.994	0.998	0.997	0.998	0.999

Table 6. Percentage of parameter sets selected as behavioral using LoAs as constraints. Total number of tested parameter sets were 10^6

Gauge	**Using 99.5^{th} percentile as upper LoA**			**Using 97.5^{th} percentile as upper LoA**		
	Gauged-single	Gauged	Ungauged	Gauged-single	Gauged	Ungauged
Allowing 5% outliers						
04180500	5.51	7.01	22.40	1.95	2.26	15.29
04180000	6.15	6.92	30.47	1.56	1.78	18.08
04179520	11.99	7.92	28.88	4.22	2.21	17.93
04178000	11.20	6.58	21.61	6.66	2.37	12.96
Without allowing outliers						
04180500	0.09	0.011	1.56	0.00	0.00	0.45
04180000	0.03	0.006	1.73	0.0001	0.00	0.37
04179520	0.16	0.004	1.57	0.003	0.00	0.30
04178000	1.75	0.009	0.94	0.50	0.00	0.22

4.2 Analysis of gauged-single scenario (LoA_{GS})

Fig. 3 shows the calibration and validation period NSEs for the behavioral models determined using LoA_{GS}. The parameter sets that satisfied the four criteria listed above during the calibration period were accepted as behavioral; the performance of behavioral parameter sets was then evaluated using the independent validation period. When 5% outliers were allowed, several models were accepted as behavioral. The calibration NSEs of the behavioral models ranged from less than

0 to ≈ 0.75. There were many models with a low calibration NSE but high validation NSE. Further, there were many non-behavioral models with high calibration NSE (not shown). When no outliers were allowed, a much smaller number of models were accepted as behavioral. Again, both calibration and validation NSEs ranged from 0 to 0.70. These results emphasize the importance of explicit consideration of uncertainties in the data for evaluating hydrological models; GoF measures such as NSE may be misleading as the models with high NSE values may still have large number of time steps inconsistent with the observations.

Figure 3 shows the behavioral models accepted using 99.5th percentile as the upper LoAs. The same plot but using 97.5th percentile as the upper LoAs is shown in Fig. S2 (SI). As expected, the plot with 97.5th percentile as the upper LoA yielded fewer behavioral models.

Figure 4 shows the scatter plot of likelihood values against NSEs for behavioral models when 5% outliers were allowed. The models with low NSEs were always assigned low likelihood values. Models with high NSEs were assigned a range of likelihood values from smallest to the largest. Thus, behavioral models with low NSE values will have very small contributions to predictive uncertainty computation, which is a desirable property. Importantly, several models with high NSE values will also have small contributions to predictive uncertainties.

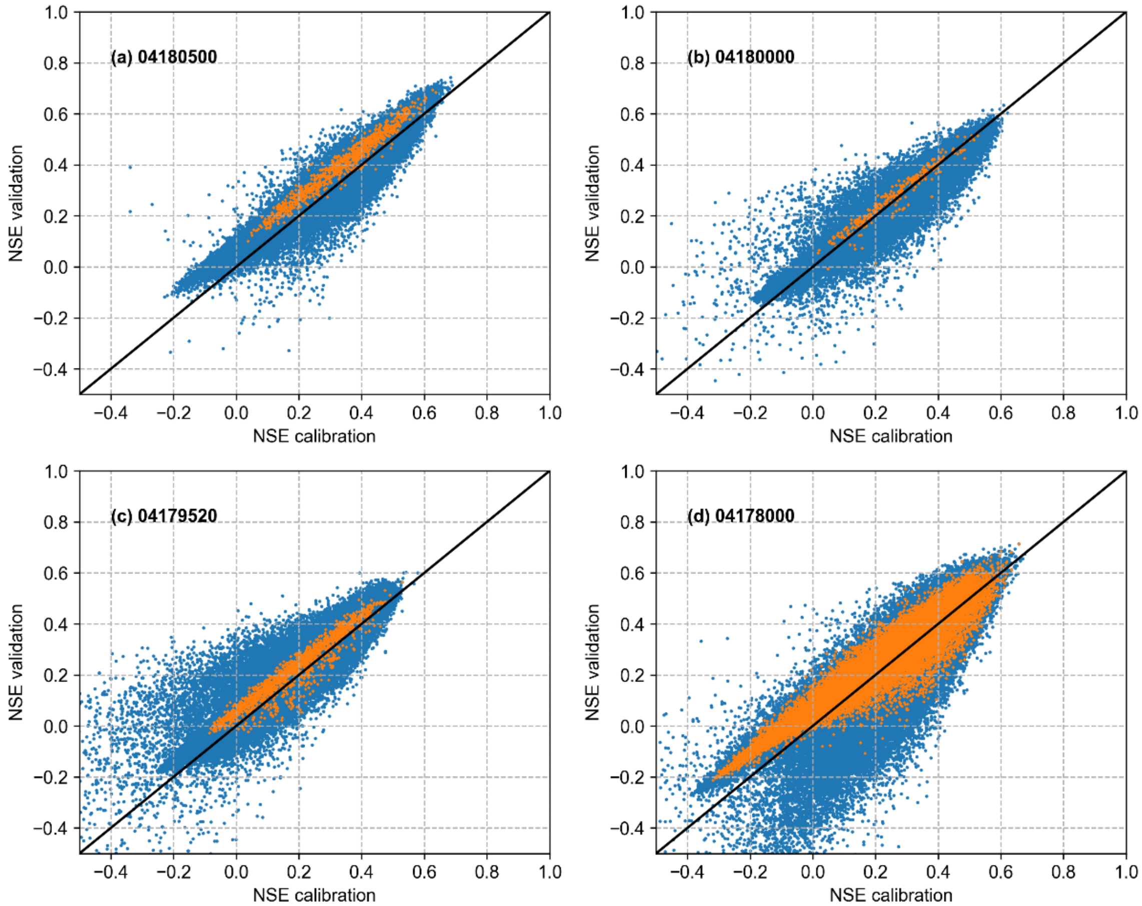

Figure 3. Using 99.5th percentile. Nash-Sutcliffe Efficiency (NSE) in calibration and validation periods for all the behavioral parameter sets obtained using limits-of-acceptability (LoA) in the gauged-single scenario. The blue markers represent the parameter sets obtained by allowing 5% outliers and the orange markers represent the parameter sets without allowing any outliers.

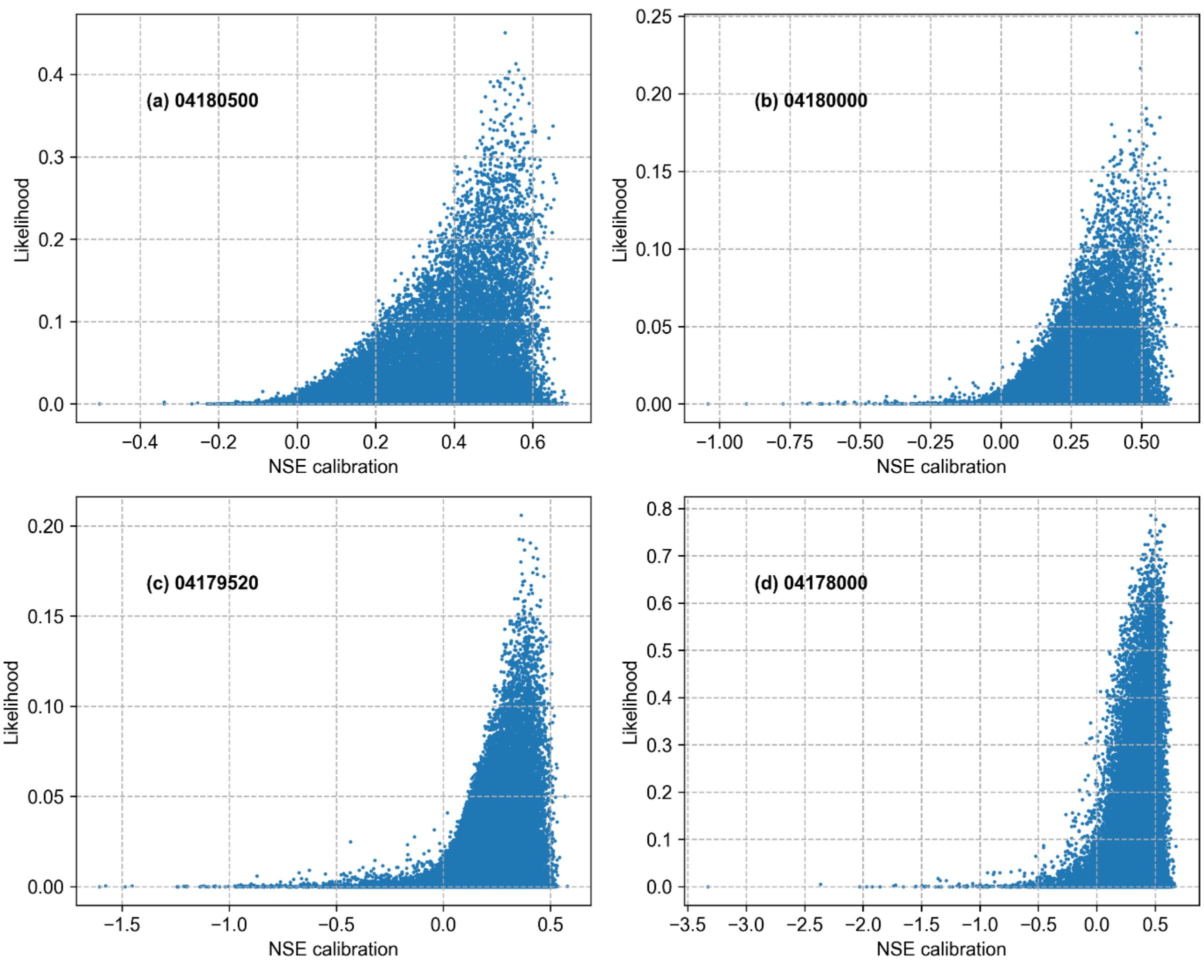

Figure 4. Using 99.5th quantile as upper LoA and allowing 5% outliers. Likelihood values plotted against calibration NSEs. Each dot represents one parameter se and the likelihood values shown are unscaled.

To further investigate the properties of the behavioral models, the observed streamflows were divided into seven ranges based on where they fall on a flow duration curve. These ranges are 0-5 percentiles, 5-20 percentiles, 20-40 percentiles, 40-60 percentiles, 60-80 percentiles, 80-95 percentiles, and 95-100 percentiles. Figure 5 shows the score values (Eq. 1) assigned to different behavioral simulations for the seven streamflow ranges at gauge 04180500. The width of the shaded part is proportional to the probability density of scores. The low flows were overestimated while the high flows were underestimated by most of the behavioral models. This general pattern was more pronounced when no outliers were allowed, implying that the several additional models accepted by allowing for outliers underestimated low flows and overestimated high flows.

The median values and shaded high-density regions were close to score zero for 0-60 percentile ranges, implying several behavioral models simulated streamflows close to the observed streamflow for these flow ranges. The median values and high-density regions were in negative score range for 60-100 percentile ranges, implying most of the behavioral models underpredicted high flows. Indeed, when no outliers were allowed, all the behavioral models underpredicted flows in the 95-100 percentile range. The results for the other three streamgauges were also similar, as shown in SI (Fig.s S3-S5).

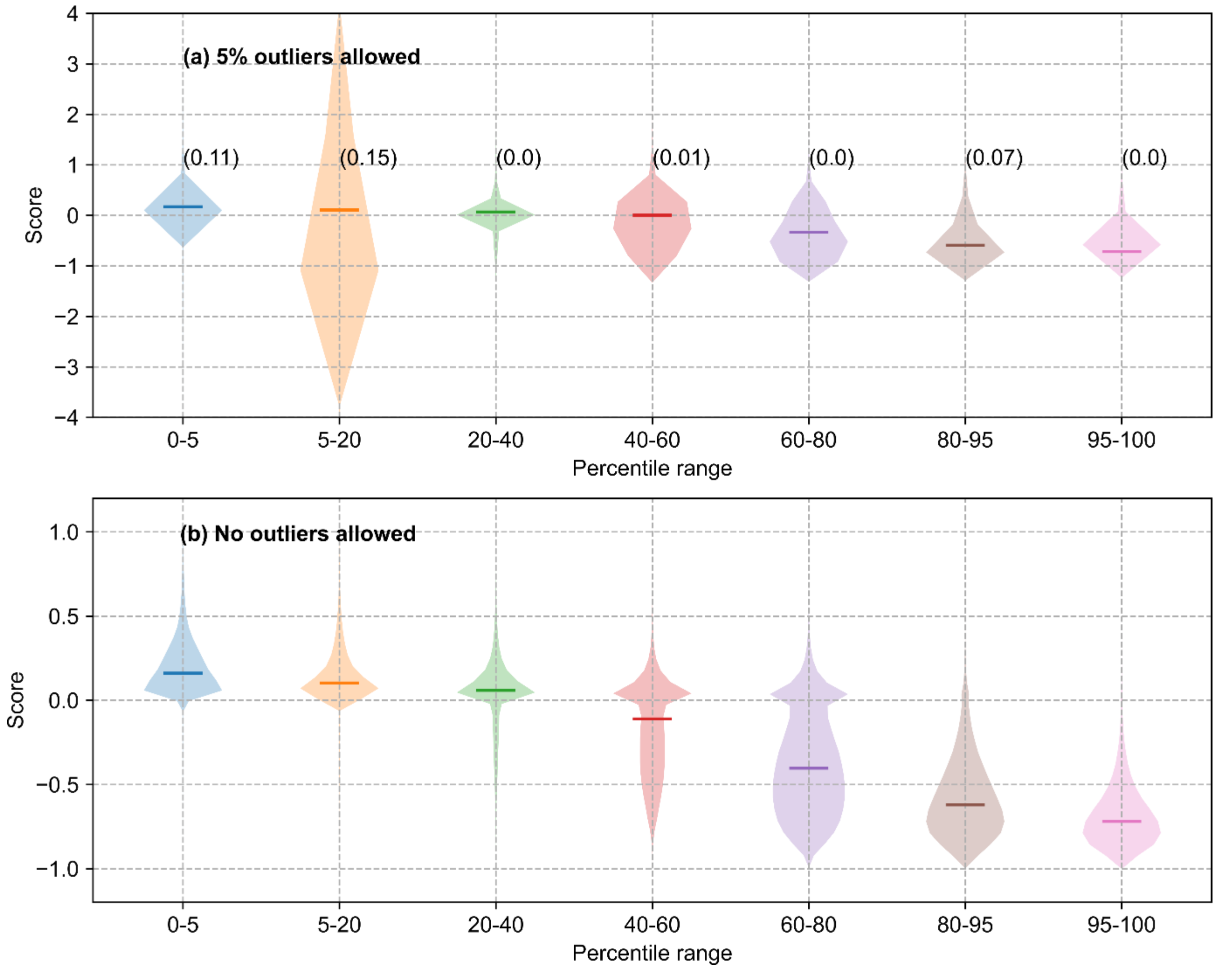

529 **Figure 5. Gauge 04180500, using 99.5th percentile as upper LoA, gauged-single scenario, and calibration period. The violin plots of score values for different percentile ranges of streamflow. The numbers in bracket in the subplot (a) are the percentage (not fraction) of simulated flow values with absolute score values greater than 4. The horizontal bar represents the median value.**

Figure 6 shows 99% credible regions (CR) for calibrations and validation periods for the gauge 04180500, for the cases of 5% outliers allowed (CR5) and no outliers allowed (CR0). As expected, the CR5 was wider than CR0 at all the timesteps. Most of the observations were enveloped by both the CRs. Some observations were not enveloped by CR0 but were enveloped by CR5; also, some observations were missed by both the CRs. At several peak flow timesteps, observations were very close to upper bounds of CR, especially in the case of CR0 because most of the behavioral models underpredicted the high flows as discussed above.

At some peak flow timesteps, there was a timing error between observed and predicted streamflows which might be either due to model deficiency or due to errors in precipitation timing. For example, at timesteps 1525, 1571, 1628, 1640, 1656, and 1661 during the validation period (Fig. 6b), observed streamflows peaked one day before the simulated streamflow peaks. Also, there was no lag between precipitation peak and observed streamflow peak at these timesteps, implying timing errors in the validation phase are likely due to model deficiencies. Such errors were fewer in the calibration period. However, there were many timesteps with one day lag between precipitation and observed streamflow likely because of timing errors in precipitation data (Gupta et al., 2023a). Since the LoA_{GS} used to select behavioral models were defined using data only from the parent watershed, they cannot capture the effect of these consistent timing errors. Thus, some of the behavioral models obtained using the LoA_{GS} are likely to overfit the calibration data. The CRs for the other three gauges are shown in Figs. S6-S8, which were similar to those shown in Fig. 6.

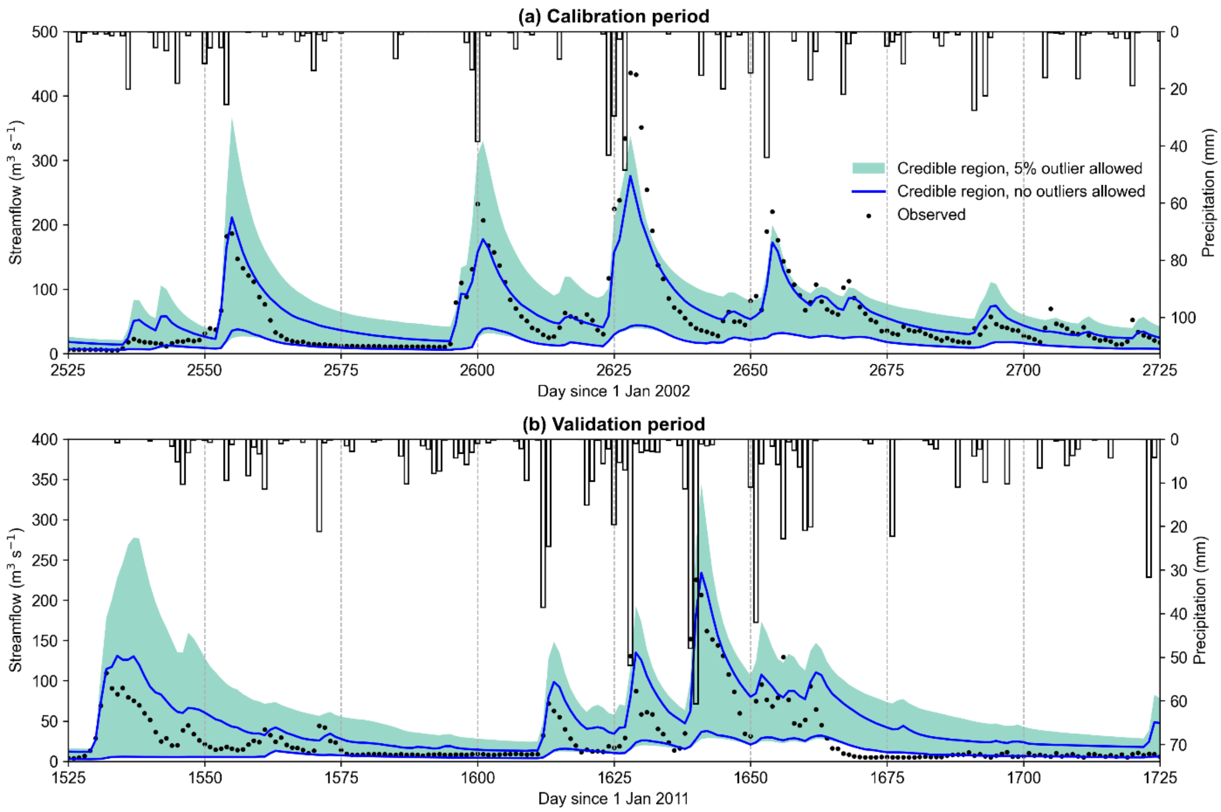

Figure 6. Gauge 04180500, using 99.5th percentile as upper LoA, and gauged-single scenario. Credible region of streamflow during calibration and validation periods obtained by allowing 5% outliers (green band) and no outliers (blue lines).

4.3 Analysis of gauged scenario

Figure 7 shows the score values (Eq. 1) assigned to different behavioral simulations and different timesteps for the seven streamflow ranges at gauge 04180500 using LoA_G to determine behavioral models. These plots are similar to those shown in Fig. 4 for gauged-single scenario with one difference. When 5% outliers were allowed, both underestimations and overestimations of observed high flows occurred in proportionate manner, while underestimations were more frequent by using LoA_{GS} (as most of the probability mass is below zero in violin plots) suggesting streamflow credible regions will be wider in gauged scenario than those in gauged-single scenario.

Figure 8 shows the 99% CRs for gauge 04180500 in the case of allowing (CR5) and not allowing outliers (CR0). Again, CRs shown in Fig. 8 are very similar to those in Fig. 5 except for one main difference. The CR5 bounds in gauged scenario (Fig. 8) were significantly wider than the CR5 bounds in gauged-single scenario (Fig. 6), as speculated above. The difference between LoA_{GS} and LoA_{G} was at the peak timesteps where LoA_{G} were wider than LoA_{GS} (Fig. 2). Consequently, CR5 bounds obtained in gauged scenario are more conservative than the CR5 bounds obtained in the gauged-single scenario. Thus, it appears information contained in data from other watersheds may be used to inform the model validation procedure in a particular watershed, as it provides slightly wider CR5 bounds compared to gauged-single scenario bands.

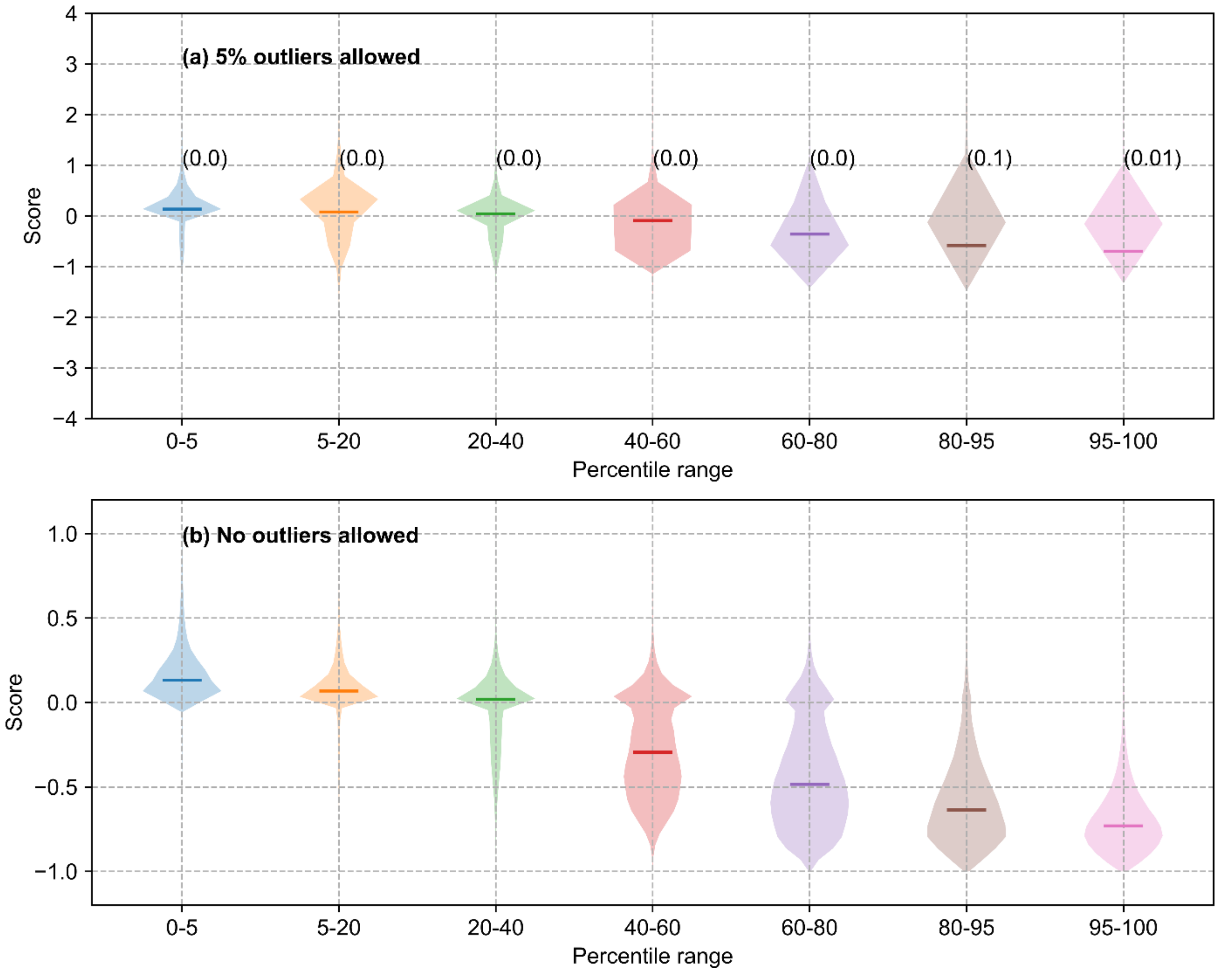

Figure 7. Gauge 04180500, using 99.5th percentile as upper LoA, and gauged scenario. The violin plots of calibration period score values for different percentile ranges of streamflow. The numbers in bracket in the subplot (a) are the percentage of simulated flow values with absolute score values greater than 4. The horizontal bar represents the median value.

The timing errors discussed in the context of gauged-single scenario are also present in the gauged scenario. The LoA_G could not help in addressing the problem of timing errors, suggesting that the model structure itself might be deficient in terms of reproducing peakflow timing. The credible region plots for the other three gauges are shown in Figs. S12-S14 (SI).

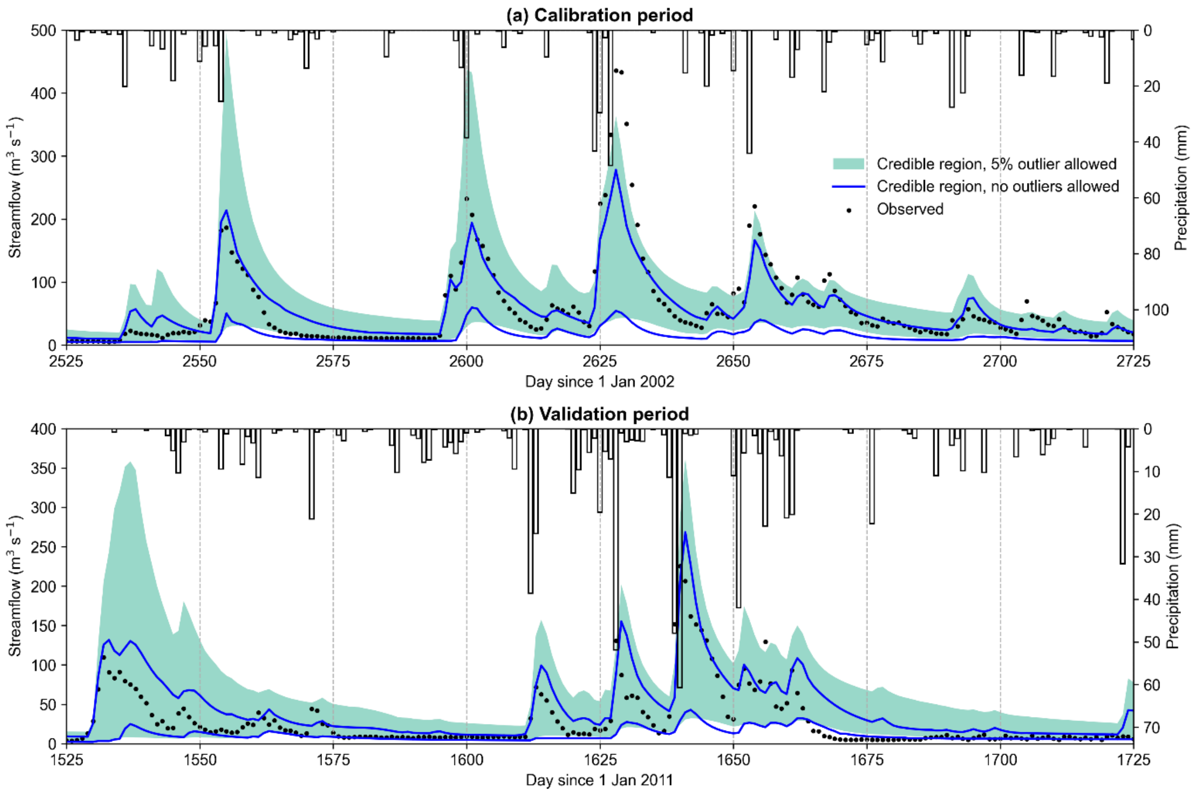

Figure 8. Gauge 04180500, using 99.5th percentile as upper LoA, and gauged scenario. Credible region of streamflow during calibration and validation periods obtained by allowing 5% outliers and no outliers.

4.4 Usefulness of streamflow signature for constraining the simulations in gauged-single and gauged scenarios

Figure 9a shows the percentage of behavioral models accepted after constraining the models by various streamflow-based signatures, for the gauged-single scenario. Clearly, all the signatures identified some models as non-behavioral that were identified as behavioral by the LoA constraint alone. The signature BFI had the most discriminating power, as using both LoA and BFI as the constraints resulted in the least number of behavioral models. The signatures ACF and H also had significant discriminating power. Similar discriminating power of ACF and H is surprising since a very relaxed condition was applied on simulated H values for a simulation to be accepted as behavioral. A likely cause is that the ACF was calculated only for first 100-day lags which does not actually contain significant information about the long-range memory, as is represented by H.

Applying all the constraints simultaneously resulted in a very small number of behavioral models. The calibration and validation NSEs for the behavioral models obtained by applying all the constraints are shown in Figs. 9b-9e. Surprisingly, the NSE values still ranged from less than 0 to greater 0.50 even for this much smaller set of models. Nevertheless, applying signature-based constrains reveals that several streamflow simulations obtained by applying the LoA constraint alone, while acceptable overall, were not simulating specific aspects of streamflow hydrographs satisfactorily. The results were similar for the gauged scenario (Fig. S15, SI).

Figure 10a compares the 99% credible region over streamflow with LoA only constraint (CRL) and with all the constrains (CRLS), for the station 04180500.Generally, CRLS were narrower than CRL but the CRLS were wider at a few time-steps. CRLS enveloped the observations at most of the time steps. There were timing errors between observed peaks and the peaks in CRLS, perhaps because none of the signatures investigated here have a strong emphasis on peak timing. The results were similar for other stations except that the timing errors were infrequent (Figs. S16-S18, SI). The CRLS were constructed with a very small number of simulations; therefore, the relevancy of these bands is questionable. It is remarkable that most of the observations could be enveloped even by these small number of behavioral simulations. But some of the peak values were missed by the CRLS, suggesting that SAC-SMA may be limited for peak flow simulations in SJRW.

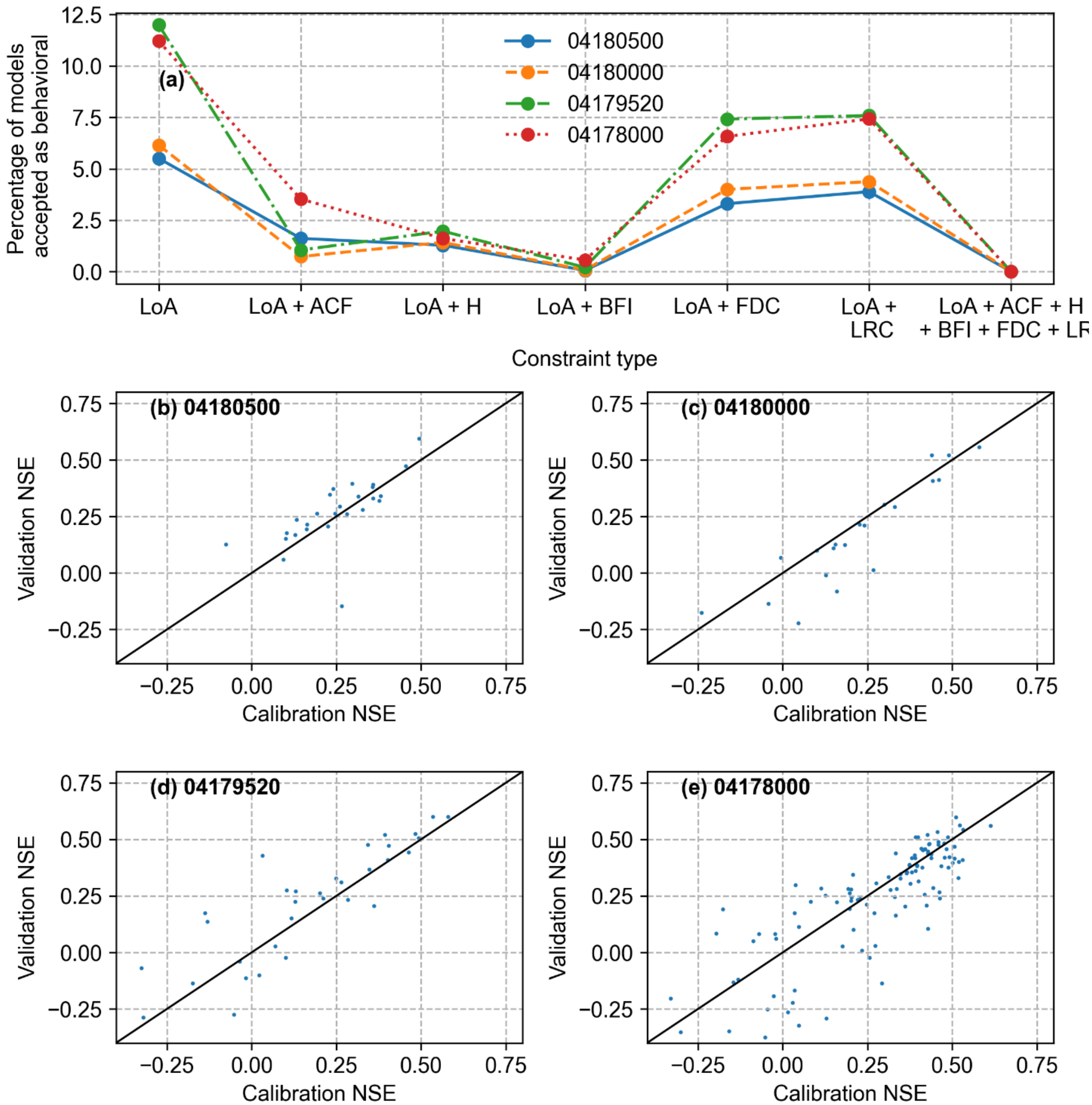

Figure 9. Gauged-single scenario and allowing 5% outlier. (a) Percentage of models accepted as behavioral, obtained by applying different constraints; (b), (c), (d) and (e) calibration and validation NSEs for the behavioral models obtained by applying all the constraints.

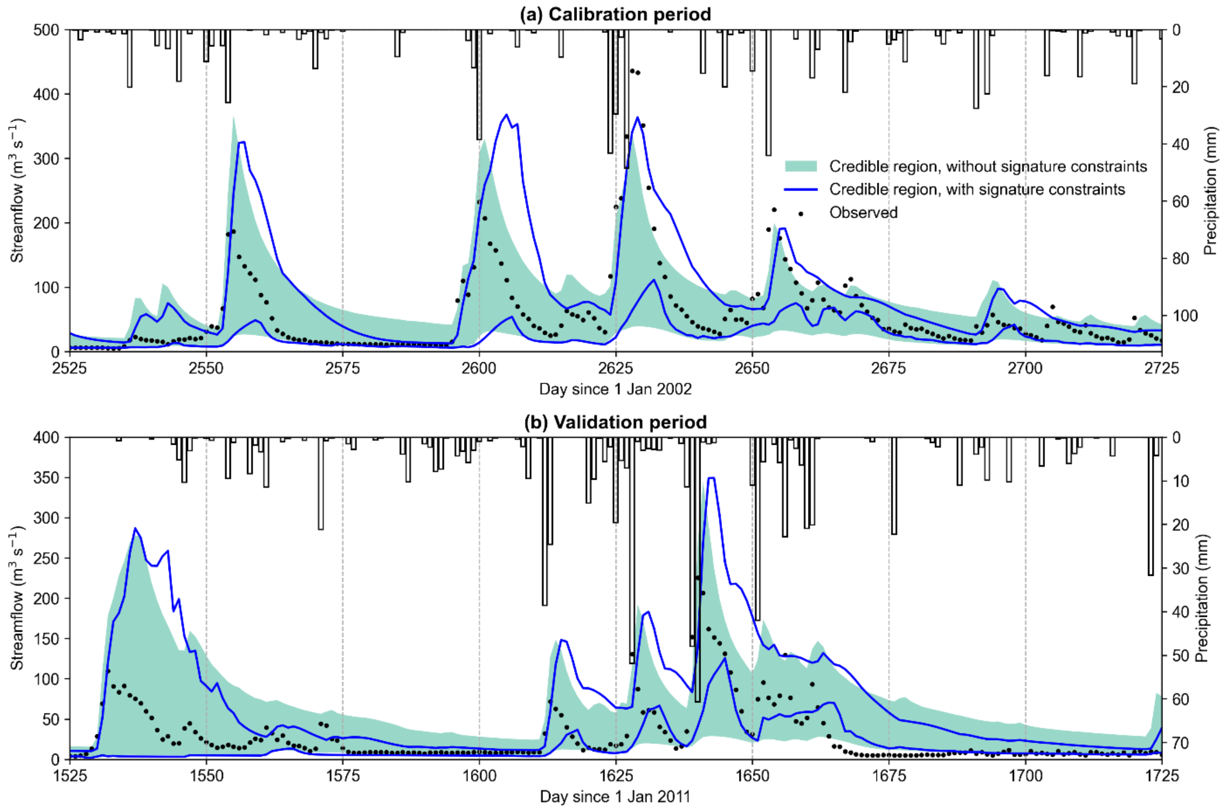

Figure 10. Gauge 04180500, using 99.5th percentile as upper LoA, and gauged-single scenario. Credible region of streamflow during calibration and validation periods obtained by allowing 5% outliers when the model was constrained only using LoAs (green band) and when the model was constrained using LoA and other constraints (blue band).

4.5 Analysis of ungauged scenario

Figure 11a shows the percentage of behavioral models accepted by using different constraints for LoA_{UG} scenario. A large number of models were accepted as behavioral when only LoA were used as constraints. The number of behavioral models reduced significantly when H or BFI were used as additional constraints. Note that very relaxed criterion for H and BFI were used in this case.

Only the models that simulated BFI less than 0.10 or greater than 0.90 were rejected as non-behavioral according to this criterion because the range of BFI values (as shown in Table 2) cannot be obtained without streamflow observations (as in ungauged scenario). Similarly, models that simulated streamflow with H value less than 0.5 or greater than 1.0 were rejected. Figures 9b-9e show calibration and validation NSEs of the behavioral models obtained after applying all the constraints. Even after applying all the constraints a large number of models were accepted as behavioral, implying a larger uncertainty is associated with prediction in ungauged basins than in gauged basins. The NSE of the behavioral models ranged from negative to strong positive values.

Figure 12 shows the 99% credible regions when model evaluation was done using LoA constraints only (CRL) and using both LoA and signature constraints (CRLS); similar plots for other stations are shown in SI (Figs. S19-S21). Both CRL and CRLS enveloped most of the observations. Interestingly, CRLS were wider than CRL at most of the timesteps even though CRLS were created using much smaller number of simulations. Even with all the constraints, the simulated streamflows had the same range (Fig. 13). Further, when only the LoA constraints were applied, many low streamflow simulations received high likelihood. Thus, even after applying all the constraints the uncertainty in streamflow prediction did not decrease, though the number of behavioral models reduced significantly. Further, the predictive uncertainty band is quite wide in this scenario. These results illustrate the challenge associated with prediction at ungauged basins.

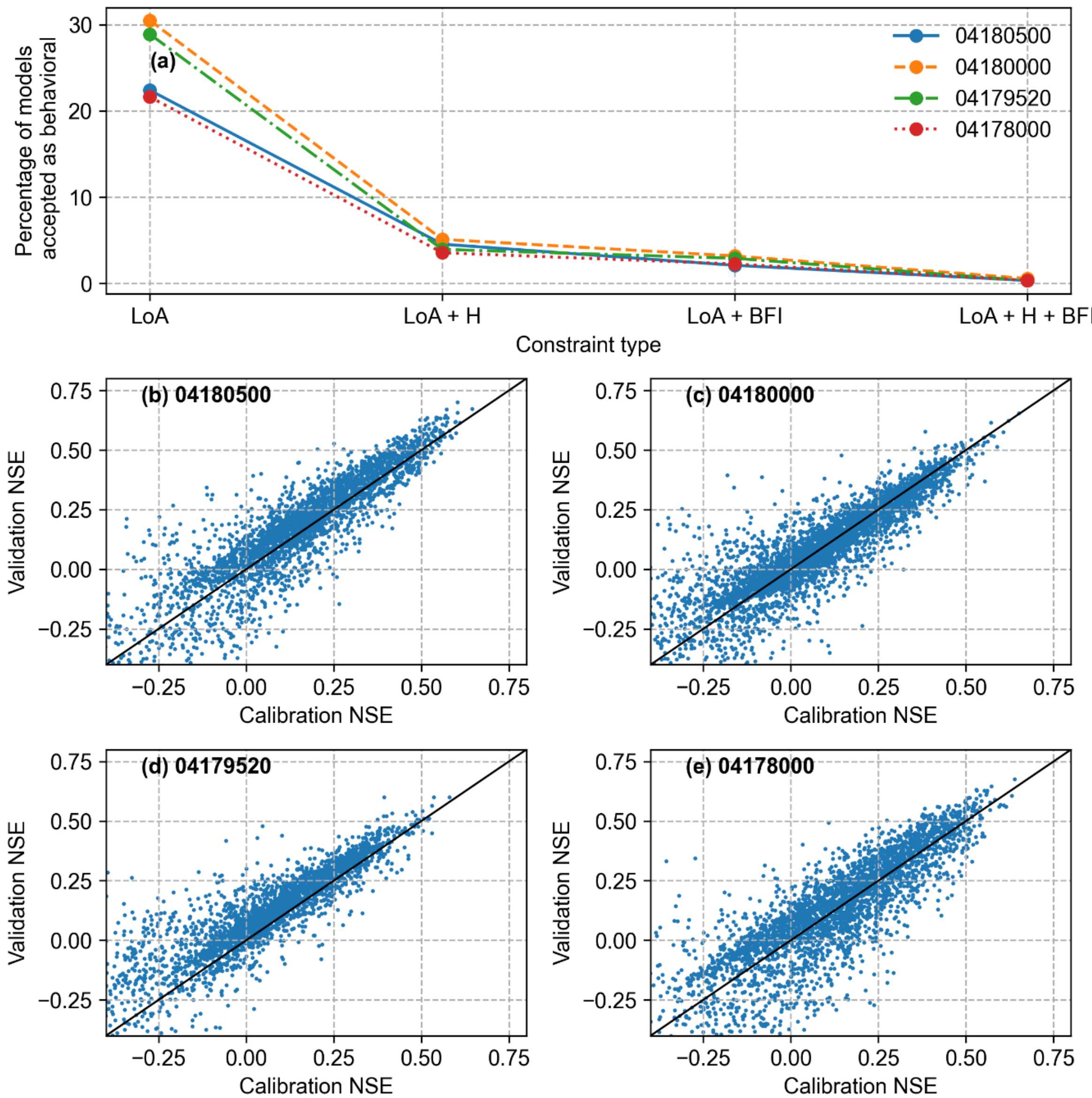

647 **Figure 11. Ungauged scenario and allowing 5% outliers. (a) Percentage of models accepted**
648 **as behavioral, obtained by applying different constraints; (b), (c), (d) and (e) calibration and**
649 **validation NSEs for the behavioral obtained by applying all the constraints.**

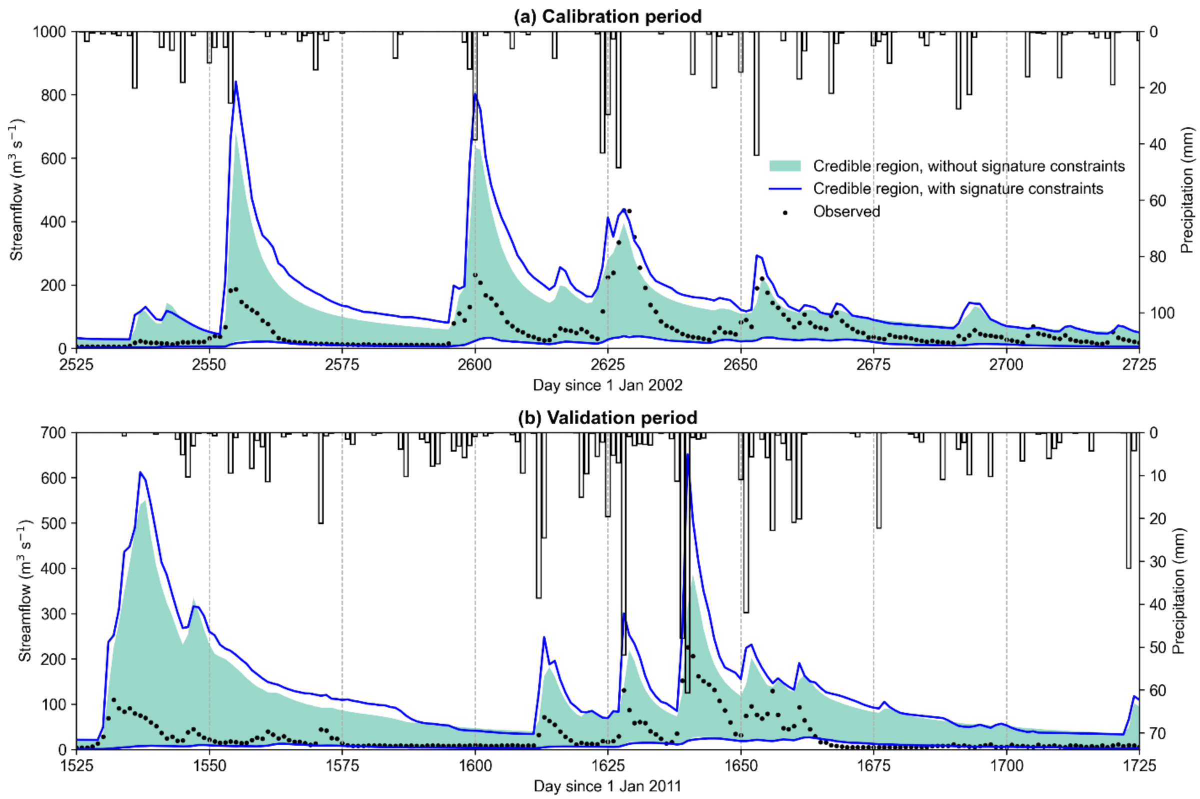

652 **Figure 12. Gauge 04180500, using 99.5th percentile as upper LoA, and ungauged scenario.**
653 **Credible region of streamflow during calibration and validation periods obtained by**
654 **allowing 5% outliers when the model was constrained only using LoAs (green band) and**
655 **when the model was constrained using LoA and other constraints (blue band).**

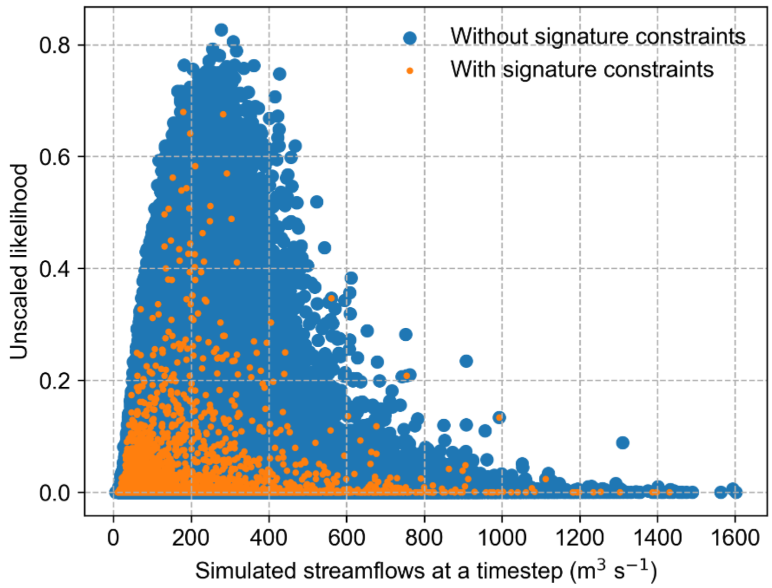

Figure 13. Gauge 04180500, using 99.5th percentile as upper LoA, ungauged scenario, and allowing 5% outliers. Likelihood vs streamflow at a particular timestep for the model constrained using LoA and LoA plus signatures.

4.6. Range of hydrological behaviors exhibited by the behavioral models

Table 7 list the range of BFI, LRC, and H values obtained by streamflow simulations deemed behavioral after applying all the constraints. These signatures reflect the hydrological behaviors possible simulated by the model. Table 7 shows that the models accepted as behavioral simulate a very wide range of hydrological behaviors, even in gauged-single scenario. This implies that even though the methodology implemented in this study identified a few models as behavioral, we could not learn much about the dominant hydrological processes in the SJRW beyond what was already assumed before using the SAC-SMA model.

Table 7. Allowing 5% outliers and using 99.5th percentile as upper LoA. Range of signatures indices corresponding to behavioral streamflow simulations obtained after applying all the constraints

Signature	Gauged-single scenario				Ungauged scenario			
	04180500	**04180000**	**04179520**	**04178000**	**04180500**	**04180000**	**04179520**	**04178000**
BFI	0.27-0.52	0.27-0.56	0.32-0.59	0.35-0.76	0.10-0.90	0.10-0.90	0.10-0.90	0.10-0.90
LRC	0.24-0.42	0.25-0.48	0.24-0.48	0.23-0.54	0.05-0.93	0.05-0.95	0.05-0.95	0.04-0.78
H	0.70-0.99	0.66-0.97	0.71-1.00	0.68-1.00	0.51-1.00	0.51-1.00	0.52-1.00	0.51-1.00

5. Discussion

This paper presented an application of QRF-based LoA in evaluating the hydrological model SAC-SMA, where the LoA were defined for streamflow time series. This allowed the evaluation of models (i.e., parameter sets of the model structure) individually for each time step. A total of 10^6 parameters sets were sampled from the prior parameter ranges. This is perhaps a small set given that the total number of free parameters was 24. Thus, it is likely that many behavioral models were missed due to sparse sampling. However, useful insights could be obtained using this set. Further, five streamflow-based signatures were used along with LoA to reject the models that could simulate streamflow within the LoA bounds but still could not reproduce specific aspects of streamflow dynamics.

Two of the subjective choices associated with the QRF-based LoA method are: (1) What quantiles should be used to define the lower and upper LoA bounds, and (2) how many and how should the outliers be allowed. Allowance for outliers is required because of the finite amount of data used to define LoAs and the dominance of epistemic errors in hydrological data (Beven and Lane, 2019;

Gupta et al., 2023a). It is possible that a model simulates low and medium flows well but provides consistently poor simulations of a few high flows observed in the calibration period. Thus, a poor model might be accepted if allowance for outliers is not made carefully. We selected outliers in a manner that a model is accepted as behavioral only if it simulates all parts of the streamflow time series (rising limb, recession limb, and peaks) consistent with observations. There can be other ways of allowing for outliers, depending on the purpose of the modeling exercise and available information about the uncertainties in data. The lower limit of the LoAs (Fig. 2) was very small (close to zero) at most of the timesteps which is because of using 1st percentile in the leaf node as the lower LOA. Consequently, these LoAs were biased toward accepting a model with underpredictions because simulated streamflows are bounded below by zero. Other percentiles can be used to define tighter LoAs; however, LoAs thus defined exclude many of the low flow observations. Therefore, perhaps, the best strategy is to use different percentiles for different parts of streamflow time series – this can be explored in future studies.

The behavioral models produced calibration and validation NSE values ranging from less than 0 to greater than 0.70 (Figs. 3, 9, and 11). Uncertainties in hydrological data were so large that several the models with poor NSE values could not be rejected. On the other hand, many models with high NSE values were rejected (not shown), implying that these models had several timesteps where streamflows were simulated outside the LoA. These results indicate that the NSE metric (or any other GoF measure for that matter) cannot capture the effects of uncertainties encountered in hydrological data. Similarly, Beven et al. (2022) rejected all the parameter sets of TOPMODEL after applying all the constraints, even though the NSE values of several rejected models were quite strong. Beven et al. (2022) defined LoA using runoff ratio method that accounts for both precipitation and streamflow uncertainties, and these authors also allowed for timing errors. Thus, these results suggest a departure from using widely used GoF measures alone as model evaluation criterion, in line with previous studies (e.g., Beven, 2019; McMillan, 2021). Gupta et al. (2008) also suggested a similar shift in model evaluation practice, specifically emphasizing the role of multiple hydrological signatures in model evaluation. As shown in this study, the uncertainty in precipitation (and possibly other inputs) and streamflow must also be considered explicitly in any model evaluation procedure, otherwise the chances of rejecting a good model are significant as several behavioral models accepted in this study had low NSE values. The LoAs defined by QRF method can account for the effects of both the precipitation and streamflow measurement uncertainties by grouping similar predictor variables in a leaf node. Note that we do not suggest that NSE should not be used at all; it is a useful measure that gives us an idea about how well the simulations fit the observations. But it should be kept in mind that a worse fit does not mean a worse model.

A large number of models were accepted as behavioral, especially when 5% outliers were allowed, for all the three LoA scenarios. This is different from some earlier studies where all the tested models were rejected using the LoA method (e.g., Liu et al., 2009; Hollaway et al., 2018). Most of these studies defined LoAs based only on streamflow uncertainty and neglected precipitation uncertainty; however, these studies artificially expanded the LoAs to identify some behavioral models. Large expansions of LoAs were usually required to obtain a meaningful number of behavioral models. In this study, no such expansions were required to identify at least some behavioral models, even when no outliers were allowed. While different models and different watersheds have been used in other studies, it can be expected that neglect of uncertainty in precipitation data might be the reason that no behavioral models were identified in the earlier studies. Further, it appears that if we had used more signatures for model evaluations in gauged-single and gauged scenarios, all the models would have been eventually rejected in this study as well.

An important question is whether a model producing an NSE of less than 0.5 should be used at all in practical applications, even though the model evaluation procedure suggests that the model is behavioral. The NSE produced by a model can be poor because of errors in data or because of inadequate model structure. The use of additional constraints on accepted model behaviors in the form of streamflow signatures revealed that many of the models accepted as behavioral by the LoA alone were inadequate for simulating specific signatures (Figs. 9a and 11a). But several of the behavioral models obtained even after applying all the constraints simultaneously produced poor NSEs. Figures 5 and 7 suggest that a reason for the low NSEs of behavioral models was consistent underestimation of high flows, which could have been due to underprediction of areal average precipitation (Bárdossy et al., 2022; Bárdossy and Anwar, 2023) given that only six gauges were available for the watersheds considered in this study (Fig. 1). We note that some earlier studies (e.g., Gallart et al., 2007; Shafii et al., 2015) have used NSE equal to zero as the threshold for a simulation to be considered as behavioral. We feel that while a model with low NSE could be used for deriving predictive uncertainty bound; it is not useful in practical applications where a good fit to observation is required even if the bad fit is due to bad data.

The signature-based constraints in addition to LoA constraints significantly reduced the number of behavioral models in all the three scenarios. The five signatures used in this study were: autocorrelation function (ACF) of streamflow, Hurst exponent (H), baseflow index (BFI), flow duration curve (FDC), and long-term runoff-coefficients (LRC). While all the constraints were helpful in reducing the number of behavioral models, the first three signatures (ACF, H, and BFI) were the most impactful. The signature BFI was the most useful for the four watersheds used in this study, but the importance of a signature depends upon the watershed being considered (Coxon et al., 2014). These three signatures (ACF, H, and BFI) are not independent. In principle, the ACF of the streamflow time series contains all the information required to estimate H, and ACF is also significantly impacted by the relative contribution of baseflow (Gupta et al., 2023b). The important point here is that several simulations accepted as behavioral by the LoA constraint alone produced unrealistic streamflow dynamics. Uncertainties in the hydrological data may significantly limit the constraining power of the observations if the comparison is made only between observed and predicted streamflow sequences. Fortunately, use of streamflow-based signatures as soft constraints (Seibert and McDonnel, 2002) can be helpful in constraining the possible model behaviors. Another notable point is that the width of uncertainty bands obtained in ungauged scenario with and without signature constraints were quite similar at all the time steps (Fig. 12), even though signature constraints rejected several models as physically unrealistic. This study suggests that that time domain calibration alone may not be enough and combining time domain calibration with signature domain calibration is a better strategy especially when the streamflow estimation is not the end goal of an application. For example, when the interest is further processing the simulated streamflow time series for water quality modeling such as water quality data reconstruction (e.g., Mallya et al., 2020), it is imperative that physically realistic realizations of streamflow are used.

Several earlier studies have used FDC alone (e.g., Westerberg et al., 2011) or in combination with other signatures (e.g., Fenicia et al., 2018) and have concluded FDC as a useful signature in constraining the model parameter space. The results of this study show that FDC is not very useful after time domain calibration, and other signatures taking advantage of spectral properties of the streamflow time series might be more useful. Among spectral properties, the Hurst exponent was particularly useful in this study and, therefore, should be explored in other studies with different models and in different watersheds. The results of this study in gauged scenarios (Fig. 9) indicate that all the tested models could have been rejected if more signatures were used. Ideally, we want a model to produce all the possible hydrological signatures for physical consistency, but this may not be possible because hydrological models are necessarily simplified representations of hydrological processes. Therefore, the signatures to be used in a practical application should be determined by a balance between the purpose of the modeling exercise and the uncertainty one is willing to bear.

The predictive uncertainty (PU) obtained in different scenarios enveloped the observations fairly well. As expected, the PU was higher when 5% outliers were allowed compared to when no outliers were allowed. The width of PU bounds was significantly affected by the definition of the likelihood function (results not shown). The likelihood function used in this study is only one of the ways of ranking models. There are many other possible formulations of the likelihood function and it tends to be a subjective choice. The likelihood function used in this study was based on the two criteria discussed above: (1) the models that simulate streamflow with large deviations from the observed streamflow should get lower likelihood, and (2) the timesteps at which streamflow is simulated outside and close to the defined LoA should be penalized more heavily. These two criteria still leave several choices available to be used as likelihood functions. Thus, the subjective choice of likelihood function remains a challenging problem in hydrological modeling, as it significantly affects the obtained PU bounds.

One of the primary motivations for hydrological modeling is the further the understanding of dominant hydrological processes in a watershed. The behavioral streamflow simulations obtained after applying all the constraints exhibited a wide range of hydrological behaviors (Table 7) implying that it is not possible to learn much about the hydrological processes in SJRW using SAC-SMA given the calibration data used in this study. Perhaps, using other data such as groundwater levels, soil moisture, water chemistry etc. would be useful in this context.

One question is how the LoA method is any better than the formal Bayesian method given the subjectivity of the likelihood function in both the approaches. Both the likelihood functions in the LoA method and the probabilistic likelihood function in formal Bayeisan theory cannot be verified in practice, given the non-stationarity of errors (Beven, 2016). The LoA method attempts to circumvent this problem (though not completely) by allowing for outliers. The advantage of LoA method is that it can assign zero likelihood to a model while the formal Bayesian method cannot. This is possible because the limits-of-acceptability are defined before any model runs. In the formal Bayesian method, the large discrepancy at some timesteps may be absorbed by the large variance in the error model. However, once a likelihood function is defined in the LoA framework, the calculus of formal Bayesian methods may be used to infer models (Nott et al., 2012; Sadegh and Vrugt, 2013; Vrugt and Sadegh, 2013; Vrugt and Beven, 2018; see also Kavetski et al., 2018; Fenicia et al., 2018).

One of the benefits of the DT based LoAs is that these LoAs can be constructed at ungauged locations by using data from donor watersheds – so called regionalization. Further, LoAs so constructed provide natural way of quantifying uncertainty in predictions. In this scenario, wider LoAs were obtained and, consequently, several models were accepted as behavioral. The wider LoAs are desirable since we expect that the regionalization would incur additional uncertainty in modeling. Using streamflow-based signatures (H and BFI) significantly reduced the number of behavioral models, but still several models could not be rejected (Fig. 11). The LoAs on signatures were defined rather loosely in this study but tighter limits could be defined using regionalization methods (e.g., Yadav et al., 2007). Using DTs to regionalize signatures and estimate associated uncertainty could also prove to be fruitful research direction, a topic that would be explored in future.

The LoAs obtained in gauged-single and gauged scenario were similar at many time-steps except at peak flow time-steps. The number of accepted behavioral models were of similar order in both the cases. Data from donor watersheds may add disinformation into the constructed LoAs (Beven, 2020). On the other hand, they may also be helpful in reflecting the effect of local epistemic errors (Gupta et al., 2023a; Gupta and Mckenna, 2023, preprint). Among the donor watersheds, DT would identify the ones that are similar to the parent watershed, thus, reducing the disinformation added to the LoAs constructed in this manner. But what watersheds are selected as similar depends upon the watershed's attributes used as predictors. Several watershed similarity metrics have been proposed within the context of prediction at ungauged basins (Wagener et al., 2007) which may be used to identify similar donor watersheds. This is a topic to be explored in future.

6. Concluding remarks

This study is the first attempt to use ML-constructed LoAs to evaluate the conceptual hydrological model SAC-SMA. Of note, the methodology proposed in this paper can be applied at both gauged and ungauged locations. Therefore, LoAs were constructed for both gauged and ungauged scenarios in this study. LoAs were wider for ungauged scenario as expected since transferring information from donor watersheds incurs additional uncertainty and, typically, the donor watersheds do not contain enough information to compensate for the absence of information from the parent watershed (Gupta, 2024). Uncertainties in hydrological data are such that just comparing observed and simulated streamflows (while taking account of errors) yields several models as behavioral, but without the ability to simulate specific hydrograph features adequately. Using streamflow-based signatures can help with this limitation. Thus, a combination of ML constructed LoAs over streamflows and streamflow-based signatures is recommended for model evaluation. Hurst exponent (H) was used as one of the signatures with very relaxed acceptability criterion, but it still was useful in constraining behavioral parameter space. Among other signatures, BFI (applied at both gauged and ungauged locations) and ACF (applicable at only gauged locations) also showed significant discriminating power.

Several models with poor NSEs were acceptable by the LoA criteria and several models with strong NSE were rejected by the LoA criteria. Even using all the constraints resulted in some behavioral models with poor NSEs. Most of the behavioral models resulted in underestimation of peak streamflow values and overestimation of low flow values. This implies that the information content in hydrological data, that is required for model evaluation, is reduced significantly due to uncertainties in the data. Though note that even the systematic errors in data might be informative in terms of streamflow prediction; such information may be extracted by a suitable ML algorithm (Gupta and Mckenna, 2023, preprint). The uncertainty in hydrological data should be explicitly accounted before model calibration process. Chances of both type-1 and type-2 errors are great if these uncertainties are not accounted for. Overall, this study suggests a departure from using popular goodness-of-fit measures alone for the evaluation of hydrological models.

Predictive uncertainty depends upon the likelihood function used to rank the models. Currently, there is no objective way to define LoA-based likelihood functions. Given the epistemic nature of errors and non-stationarities in errors, it is unlikely that objective likelihood functions can be derived. Therefore, the definition of likelihood functions should depend upon the purpose of modeling.

Appendix A

Estimation of baseflow and baseflow index (BFI) range:

The method of Collischonn and Fan (2013) was used to estimate baseflow. The stepwise method is as follows:

Step 1: Estimate master recession curve (MRC) by combining several recession curves (Lamb and Beven, 1997).

Step 2: Fit MRC with a log-linear (Eq. A1) and a piecewise log-linear model (Eq. A2):

$$\ln\left(\frac{Q_t}{Q_0}\right) = -at, \tag{A1}$$

$$\ln\left(\frac{Q_t}{Q_0}\right) = \begin{cases} -bt, & t \le t_1 \\ -at, & t > t_1 \end{cases}. \tag{A2}$$

The one of the two models yielding better fit (measured using Akaike Information Criterion) was chosen.

Step 3: Estimate initial baseflow q^i using the equation

$$q_t^i = \frac{q_{t+1}^i}{a}. \tag{A3}$$

Step 4: estimate a parameter denoted by BFI_{max} as follows:

$$BFI_{\mathrm{max}} = \frac{\sum_{t=1}^{T} q_t^i}{\sum_{t=1}^{T} Q_t}. \tag{A4}$$

Step 5: Obtain another estimate of baseflow by using the Eckhardt filter (Eckhardt, 2005):

$$q_t^1 = \frac{(1 - BFI_{\mathrm{max}})aq_{t-1} + (1-a)BFI_{\mathrm{max}}Q_t}{1 - a\,BFI_{\mathrm{max}}}. \tag{A5}$$

The estimate q^1 was used to compute another value of BFI denoted by BFI_1.

Step 6: Repeat step 5 but by using BFI_1 in place of $BFI_{\max}$. This yielded another estimate of BFI denoted by BFI_2.

Step 7: Repeat step 5 iteratively by using latest value of BFI in place of $BFI_{\max}$. Iterations are carried out until the BFI converges.

Thus, this method yields a range of values of BFI.

Code availability

Codes used in this study will be made available upon request to the corresponding author.

Data availability

The data produced in this manuscript are available at Gupta et al. (2024a, 2024b, 2024c, 2024d, 2024e, 2024g, 2024h)

Author contribution

AG: Conceptualization, Data curation, Formal analysis, Investigation, Methodology, Software, Validation, Visualization, Writing – original draft preparation

MMH: Conceptualization, Supervision, Validation, Writing – review and editing

RSG: Conceptualization, Supervision, Validation, Writing – review and editing

Competing interests

The authors declare that they have no conflict of interest.

Disclaimer

The views expressed in this article are those of the author(s) and do not necessarily represent the views or policies of the U.S. Environmental Protection Agency.

Acknowledgements

AG was supported by Institute Project Assignment funds of Desert Research Institute and Maki postdoctoral fellowship during the performance of this work. This support is gratefully acknowledged. The idea of this project originated from another project supported by United States Environmental Protection Agency. This support is also acknowledged.

References

Anderson, E. A. (1976), A point energy and mass balance model of a snowcover, NOAA Tech. Rep. NWS 19, 150 pp., Natl. Oceanic and Atmos. Admin., Silver Spring, Md

Bárdossy, A., & Anwar, F. (2023). Why do our rainfall–runoff models keep underestimating the peak flows? Hydrology and Earth System Sciences, *27*(10), 1987-2000.

Bárdossy, A., Kilsby, C., Birkinshaw, S., Wang, N., & Anwar, F. (2022). Is precipitation responsible for the most hydrological model uncertainty? Frontiers in Water, 4, 836554.

Beran, J. (1994). Statistics for long-memory processes (Vol. 61). CRC press.

Beven, K. (2006). A manifesto for the equifinality thesis. Journal of Hydrology, 320(1-2), 18-36.

Beven, K. (2016). Facets of uncertainty: epistemic uncertainty, non-stationarity, likelihood, hypothesis testing, and communication. Hydrological Sciences Journal, 61(9), 1652-1665.

Beven, K. (2019). Towards a methodology for testing models as hypotheses in the inexact sciences. Proceedings of the Royal Society A, 475(2224), 20180862.

Beven, K. (2023). Benchmarking hydrological models for an uncertain future. Hydrological Processes, e14882.

Beven, K., & Binley, A. (1992). The future of distributed models: model calibration and uncertainty prediction. Hydrological Processes, 6(3), 279-298.

Beven, K., & Lane, S. (2019). Invalidation of models and fitness-for-purpose: A rejectionist approach. Computer simulation validation: Fundamental concepts, methodological frameworks, and philosophical perspectives, 145-171.

Beven, K., & Smith, P. (2015). Concepts of information content and likelihood in parameter calibration for hydrological simulation models. Journal of Hydrologic Engineering, 20(1), A4014010.

Beven, K., & Westerberg, I. (2011). On red herrings and real herrings: disinformation and information in hydrological inference. Hydrological Processes, 25(10), 1676-1680.

Beven, K., Lane, S., Page, T., Kretzschmar, A., Hankin, B., Smith, P., & Chappell, N. (2022). On (in) validating environmental models. 2. Implementation of a Turing-like test to modelling hydrological processes. Hydrological Processes, 36(10), e14703.

Burnash, R. J. C. (1995). The NWS River Forecast System-catchment modeling. Computer models of watershed hydrology., 311-366.

Castiglioni, S., Lombardi, L., Toth, E., Castellarin, A., & Montanari, A. (2010). Calibration of rainfall-runoff models in ungauged basins: A regional maximum likelihood approach. Advances in Water Resources, 33(10), 1235-1242.

Collischonn, W., & Fan, F. M. (2013). Defining parameters for Eckhardt's digital baseflow filter. Hydrological Processes, 27(18), 2614-2622.

Coxon, G., Freer, J., Wagener, T., Odoni, N. A., & Clark, M. (2014). Diagnostic evaluation of multiple hypotheses of hydrological behaviour in a limits-of-acceptability framework for 24 UK catchments. Hydrological Processes, *28*(25), 6135-6150.

Dal Molin, M., Kavetski, D., Albert, C., & Fenicia, F. (2023). Exploring Signature-Based Model Calibration for Streamflow Prediction in Ungauged Basins. Water Resources Research, 59(7), e2022WR031929.

De Vleeschouwer, N., & Pauwels, V. R. N. (2013). Assessment of the indirect calibration of a rainfall-runoff model for ungauged catchments in Flanders. Hydrology and Earth System Sciences, 17(5), 2001-2016.

Di Baldassarre, G., & Montanari, A. (2009). Uncertainty in river discharge observations: a quantitative analysis. Hydrology and Earth System Sciences, 13(6), 913-921.

Duan, Q., Sorooshian, S., & Gupta, V. (1992). Effective and efficient global optimization for conceptual rainfall-runoff models. Water Resources Research, 28(4), 1015-1031.

Eckhardt, K. (2005). How to construct recursive digital filters for baseflow separation. Hydrological Processes: An International Journal, 19(2), 507-515.

Efstratiadis, A., & Koutsoyiannis, D. (2010). One decade of multi-objective calibration approaches in hydrological modelling: a review. Hydrological Sciences Journal–Journal Des Sciences Hydrologiques, 55(1), 58-78.

Euser, T., Winsemius, H. C., Hrachowitz, M., Fenicia, F., Uhlenbrook, S., & Savenije, H. H. G. (2013). A framework to assess the realism of model structures using hydrological signatures. Hydrology and Earth System Sciences, 17(5), 1893-1912.

Euser, T., Winsemius, H. C., Hrachowitz, M., Fenicia, F., Uhlenbrook, S., & Savenije, H. H. G. (2013). A framework to assess the realism of model structures using hydrological signatures. Hydrology and Earth System Sciences, 17(5), 1893-1912.

Fenicia, F., Kavetski, D., Reichert, P., & Albert, C. (2018). Signature-domain calibration of hydrological models using approximate Bayesian computation: Empirical analysis of fundamental properties. Water Resources Research, 54(6), 3958-3987.

Gallart, F., Latron, J., Llorens, P., & Beven, K. (2007). Using internal catchment information to reduce the uncertainty of discharge and baseflow predictions. Advances in Water Resources, 30(4), 808-823.

Gong, W., Gupta, H. V., Yang, D., Sricharan, K., & Hero III, A. O. (2013). Estimating epistemic and aleatory uncertainties during hydrologic modeling: An information theoretic approach. Water Resources Research, 49(4), 2253-2273.

Gupta, A. (2024). Information and disinformation in hydrological data across space: The case of streamflow predictions using machine learning. Journal of Hydrology: Regional Studies, 51, 101607.

Gupta, A., & Govindaraju, R. S. (2022). Uncertainty quantification in watershed hydrology: Which method to use? Journal of Hydrology, 128749.

Gupta, A., & McKenna, S. A. (2023). Deep Learning Models Filter Out Local Errors in Hydrological Data. EarthArxiv. Preprint

Gupta, A., Carroll, R. W., & McKenna, S. A. (2023b). Changes in streamflow statistical structure across the United States due to recent climate change. Journal of Hydrology, 620, 129474.

Gupta, A., Govindaraju, R. S., Li, P. C., & Merwade, V. (2023a). On Constructing Limits-of-Acceptability in Watershed Hydrology using Decision Trees. Advances in Water Resources, 104486.

Gupta, A., Hantush, M., & Govindaraju, R. (2024a). Evaluating a conceptual hydrological model at gauged and ungauged basins using machine learning-based limits-of-acceptability and hydrological signatures - 1 [Data set]. Zenodo. https://doi.org/10.5281/zenodo.10483643

Gupta, A., Hantush, M., & Govindaraju, R. (2024b). Evaluating a conceptual hydrological model at gauged and ungauged basins using machine learning-based limits-of-acceptability and hydrological signatures - 2 (Version 1) [Data set]. Zenodo. DOI: https://doi.org/10.5281/zenodo.10483702

Gupta, A., Hantush, M., & Govindaraju, R. (2024c). Evaluating a conceptual hydrological model at gauged and ungauged basins using machine learning-based limits-of-acceptability and hydrological signatures - 3 (Version 1) [Data set]. Zenodo. DOI: https://doi.org/10.5281/zenodo.10483938

Gupta, A., Hantush, M., & Govindaraju, R. (2024d). Evaluating a conceptual hydrological model at gauged and ungauged basins using machine learning-based limits-of-acceptability and hydrological signatures - 4 (Version 1) [Data set]. Zenodo. DOI: https://doi.org/10.5281/zenodo.10483964

Gupta, A., Hantush, M., & Govindaraju, R. (2024e). Evaluating a conceptual hydrological model at gauged and ungauged basins using machine learning-based limits-of-acceptability and hydrological signatures - 5 (Version 1) [Data set]. Zenodo. DOI: https://doi.org/10.5281/zenodo.10530454

Gupta, A., Hantush, M., & Govindaraju, R. (2024f). Evaluating a conceptual hydrological model at gauged and ungauged basins using machine learning-based limits-of-acceptability and hydrological signatures - 6 (Version 1) [Data set]. Zenodo. DOI: https://doi.org/10.5281/zenodo.10515777

Gupta, A., Hantush, M., & Govindaraju, R. (2024g). Evaluating a conceptual hydrological model at gauged and ungauged basins using machine learning-based limits-of-acceptability and hydrological signatures - 7 (Version 1) [Data set]. Zenodo. DOI: https://doi.org/10.5281/zenodo.10515763

Gupta, H. V., Wagener, T., & Liu, Y. (2008). Reconciling theory with observations: elements of a diagnostic approach to model evaluation. Hydrological Processes: An International Journal, 22(18), 3802-3813.

Hamon, W. R. (1963). Computation of direct runoff amounts from storm rainfall. Int. Assoc. Sci. Hydrol. Publ., 63, 52-62.

Harvey, N., Marshall, L., & Vervoort, R. W. (2023). Verifying model performance using validation of Pareto solutions. Journal of Hydrology, 621, 129594.

Hastie, T., Tibshirani, R., & Friedman, J. H. (2009). The elements of statistical learning: data mining, inference, and prediction (Vol. 2, pp. 1-758). New York: springer.

Hrachowitz, M., Fovet, O., Ruiz, L., Euser, T., Gharari, S., Nijzink, R., ... & Gascuel-Odoux, C. (2014). Process consistency in models: The importance of system signatures, expert knowledge, and process complexity. Water Resources Research, 50(9), 7445-7469.

Hrachowitz, M., Savenije, H. H. G., Blöschl, G., McDonnell, J. J., Sivapalan, M., Pomeroy, J. W., ... & Cudennec, C. (2013). A decade of Predictions in Ungauged Basins (PUB)—a review. Hydrological sciences journal, 58(6), 1198-1255.

Hughes, D. A., & Farinosi, F. (2021). Unpacking some of the linkages between uncertainties in observational data and the simulation of different hydrological processes using the Pitman model in the data scarce Zambezi River basin. Hydrological Processes, 35(4), e14141.

Jaynes, E. T. (2002). Probability theory: the logic of science. St. Louis, MO: Washington University.

Kavetski, D., Fenicia, F., Reichert, P., & Albert, C. (2018). Signature-domain calibration of hydrological models using approximate Bayesian computation: Theory and comparison to existing applications. Water Resources Research, 54(6), 4059-4083.

Khatami, S., Peel, M. C., Peterson, T. J., & Western, A. W. (2019). Equifinality and flux mapping: A new approach to model evaluation and process representation under uncertainty. Water Resources Research, 55(11), 8922-8941.

Kim, D. H., Rao, P. S. C., Kim, D., & Park, J. (2016). 1/f noise analyses of urbanization effects on streamflow characteristics. Hydrological Processes, 30(11), 1651-1664.

Kiraz, M., Coxon, G., & Wagener, T. (2023). A Signature-Based Hydrologic Efficiency Metric for Model Calibration and Evaluation in Gauged and Ungauged Catchments. Water Resources Research, 59(11), e2023WR035321.

Knoben, W. J., Freer, J. E., Peel, M. C., Fowler, K. J. A., & Woods, R. A. (2020). A brief analysis of conceptual model structure uncertainty using 36 models and 559 catchments. Water Resources Research, 56(9), e2019WR025975.

Kratzert, F., Klotz, D., Shalev, G., Klambauer, G., Hochreiter, S., & Nearing, G. (2019). Towards learning universal, regional, and local hydrological behaviors via machine learning applied to large-sample datasets. Hydrology and Earth System Sciences, 23(12), 5089-5110.

Krueger, T., Freer, J., Quinton, J. N., Macleod, C. J., Bilotta, G. S., Brazier, R. E., ... & Haygarth, P. M. (2010). Ensemble evaluation of hydrological model hypotheses. Water Resources Research, 46(7).

Kuczera, G., Kavetski, D., Franks, S., & Thyer, M. (2006). Towards a Bayesian total error analysis of conceptual rainfall-runoff models: Characterising model error using storm-dependent parameters. Journal of Hydrology, 331(1-2), 161-177.

Lamb, R., & Beven, K. (1997). Using interactive recession curve analysis to specify a general catchment storage model. Hydrology and Earth System Sciences, 1(1), 101-113.

Le Coz, J., Renard, B., Bonnifait, L., Branger, F., & Le Boursicaud, R. (2014). Combining hydraulic knowledge and uncertain gaugings in the estimation of hydrometric rating curves: A Bayesian approach. Journal of Hydrology, 509, 573-587.

Lindley, D. V. (2013). Understanding uncertainty. John Wiley & Sons.

Liu, Y., Freer, J., Beven, K., & Matgen, P. (2009). Towards a limits of acceptability approach to the calibration of hydrological models: Extending observation error. Journal of Hydrology, 367(1-2), 93-103.

Mai, J. (2023). Ten strategies towards successful calibration of environmental models. Journal of Hydrology, 620, 129414.

Mallya, G., Gupta, A., Hantush, M. M., & Govindaraju, R. S. (2020). Uncertainty quantification in reconstruction of sparse water quality time series: Implications for watershed health and risk-based TMDL assessment. Environmental Modelling & Software, 131, 104735.

McMillan, H. K. (2021). A review of hydrologic signatures and their applications. Wiley Interdisciplinary Reviews: Water, 8(1), e1499.

Montanari, A., & Koutsoyiannis, D. (2012). A blueprint for process-based modeling of uncertain hydrological systems. Water Resources Research, 48(9).

Montanari, A., Rosso, R., & Taqqu, M. S. (1997). Fractionally differenced ARIMA models applied to hydrologic time series: Identification, estimation, and simulation. Water Resources Research, 33(5), 1035-1044.

Montanari, A., Taqqu, M. S., & Teverovsky, V. (1999). Estimating long-range dependence in the presence of periodicity: an empirical study. Mathematical and Computer Modelling, 29(10-12), 217-228.

Mudelsee, M. (2007). Long memory of rivers from spatial aggregation. Water Resources Research, 43(1).

Nott, D. J., Marshall, L., & Brown, J. (2012). Generalized likelihood uncertainty estimation (GLUE) and approximate Bayesian computation: What's the connection? Water Resources Research, 48(12).

Pande, S. (2013a). Quantile hydrologic model selection and model structure deficiency assessment: 1. Theory. Water Resources Research, 49(9), 5631-5657.

Pande, S. (2013b). Quantile hydrologic model selection and model structure deficiency assessment: 2. Applications. Water Resources Research, 49(9), 5658-5673.

Parker, W. S. (2020). Model evaluation: An adequacy-for-purpose view. Philosophy of Science, 87(3), 457-477.

Priestley, M.B. (1982). Spectral analysis and time series: probability and mathematical statistics Academic Press (No. 04; QA280, P7.).

Razavi, T., & Coulibaly, P. (2013). Streamflow prediction in ungauged basins: review of regionalization methods. Journal of Hydrologic Engineering, 18(8), 958-975.

Refsgaard, J. C., Stisen, S., & Koch, J. (2022). Hydrological process knowledge in catchment modelling–Lessons and perspectives from 60 years development. Hydrological Processes, 36(1), e14463.

Renard, B., Kavetski, D., Kuczera, G., Thyer, M., & Franks, S. W. (2010). Understanding predictive uncertainty in hydrologic modeling: The challenge of identifying input and structural errors. Water Resources Research, 46(5).

Sadegh, M., & Vrugt, J. A. (2013). Approximate Bayesian Computation in hydrologic modeling: equifinality of formal and informal approaches. Hydrology & Earth System Sciences Discussions, 10(4).

Sadegh, M., & Vrugt, J. A. (2013). Bridging the gap between GLUE and formal statistical approaches: approximate Bayesian computation. Hydrology and Earth System Sciences, 17(12), 4831-4850.

Schaefli, B., & Kavetski, D. (2017). Bayesian spectral likelihood for hydrological parameter inference. Water Resources Research, 53(8), 6857-6884.

Seibert, J., & McDonnell, J. J. (2002). On the dialog between experimentalist and modeler in catchment hydrology: Use of soft data for multicriteria model calibration. Water Resources Research, 38(11), 23-1.

Shafii, M., & Tolson, B. A. (2015). Optimizing hydrological consistency by incorporating hydrological signatures into model calibration objectives. Water Resources Research, 51(5), 3796-3814.

Shafii, M., Tolson, B., & Matott, L. S. (2015). Addressing subjective decision-making inherent in GLUE-based multi-criteria rainfall–runoff model calibration. Journal of Hydrology, 523, 693-705.

Sorooshian, S., Duan, Q., & Gupta, V. K. (1993). Calibration of rainfall-runoff models: Application of global optimization to the Sacramento Soil Moisture Accounting Model. Water Resources Research, 29(4), 1185-1194.

Tolson, B. A., & Shoemaker, C. A. (2007). Dynamically dimensioned search algorithm for computationally efficient watershed model calibration. Water Resources Research, 43(1).

Vrugt, J. A., & Beven, K. J. (2018). Embracing equifinality with efficiency: Limits of Acceptability sampling using the DREAM (LOA) algorithm. Journal of Hydrology, 559, 954-971.

Vrugt, J. A., & Sadegh, M. (2013). Toward diagnostic model calibration and evaluation: Approximate Bayesian computation. Water Resources Research, 49(7), 4335-4345.

Vrugt, J. A., Gupta, H. V., Dekker, S. C., Sorooshian, S., Wagener, T., & Bouten, W. (2006). Application of stochastic parameter optimization to the Sacramento Soil Moisture Accounting model. Journal of Hydrology, 325(1-4), 288-307.

Wagener, T., & Montanari, A. (2011). Convergence of approaches toward reducing uncertainty in predictions in ungauged basins. Water Resources Research, 47(6).

Wagener, T., Sivapalan, M., Troch, P., & Woods, R. (2007). Catchment classification and hydrologic similarity. Geography Compass, *1*(4), 901-931.

Weijs, S. V., Schoups, G. V., & Van De Giesen, N. (2010a). Why hydrological predictions should be evaluated using information theory. Hydrology and Earth System Sciences, 14(12), 2545-2558.

Weijs, S. V., Van De Giesen, N., & Parlange, M. B. (2013). Data compression to define information content of hydrological time series. Hydrology and Earth System Sciences, 17(8), 3171-3187.

Weijs, S. V., Van Nooijen, R., & Van De Giesen, N. (2010b). Kullback–Leibler divergence as a forecast skill score with classic reliability–resolution–uncertainty decomposition. Monthly Weather Review, 138(9), 3387-3399.

Westerberg, I. K., & McMillan, H. K. (2015). Uncertainty in hydrological signatures. Hydrology and Earth System Sciences, 19(9), 3951-3968.

Westerberg, I. K., Guerrero, J. L., Younger, P. M., Beven, K. J., Seibert, J., Halldin, S., ... & Xu, C. Y. (2011). Calibration of hydrological models using flow-duration curves. Hydrology and Earth System Sciences, 15(7), 2205-2227.

Winsemius, H. C., Schaefli, B., Montanari, A., & Savenije, H. H. G. (2009). On the calibration of hydrological models in ungauged basins: A framework for integrating hard and soft hydrological information. Water Resources Research, 45(12).

Yadav, M., Wagener, T., & Gupta, H. (2007). Regionalization of constraints on expected watershed response behavior for improved predictions in ungauged basins. Advances in Water Resources, 30(8), 1756-1774.

Supplementary Information for

Evaluating a conceptual hydrological model at gauged and ungauged basins using machine learning based limits-of-acceptability and hydrological signatures

Abhinav Gupta[1*], Mohamed M. Hantush[2], Rao S. Govindaraju[3]

[1]Department of Chemical and Environmental Engineering, University of Cinicinnati
[2]Center for Environmental Solutions & Emergency Response, United States Environmental Protection Agency
[3]Lyles School of Civil Engineering, Purdue University

Contents:

Figures S1-S21

S1. Limits-of-acceptability

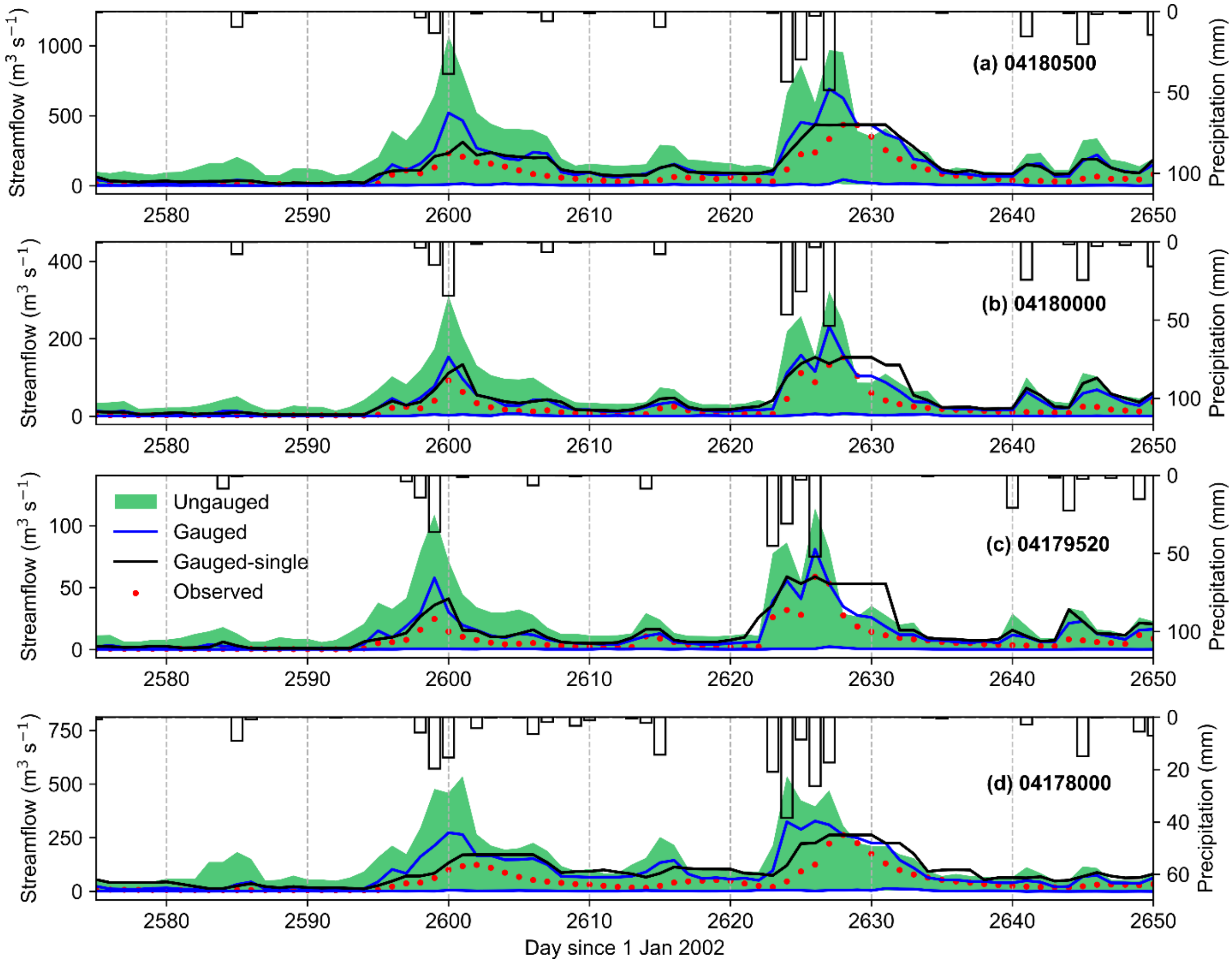

Figure S1. **Using 97.5th percentile**. Limits-of-acceptability (LoA) obtained in three scenarios: Ungauged (green band), Gauged (blue band), and Gauged-single (black band), along with observed streamflow (red dots) and precipitation. The upper LoA bounds were determined using 99.5th percentiles.

S2. Gauged-single scenario

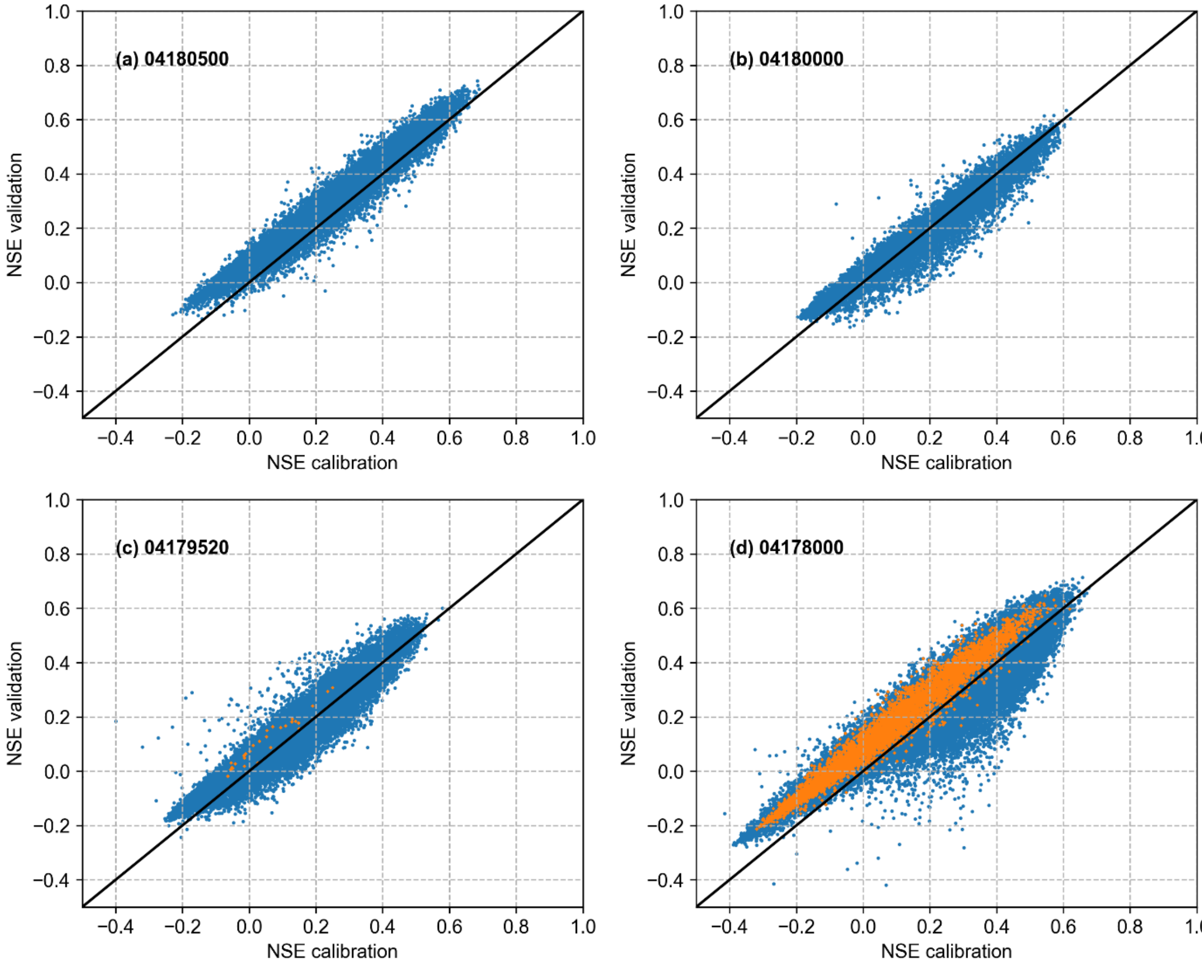

Figure S2. **Using 97.5th percentile**. Nash-Sutcliffe Efficiency (NSE) in calibration and validation periods for all the behavioral parameter sets obtained using limits-of-acceptability (LoA) in the gauged-single scenario. The blue markers represent the parameter sets obtained by allowing 5% outliers and the orange markers represent the parameter sets without allowing any outliers.

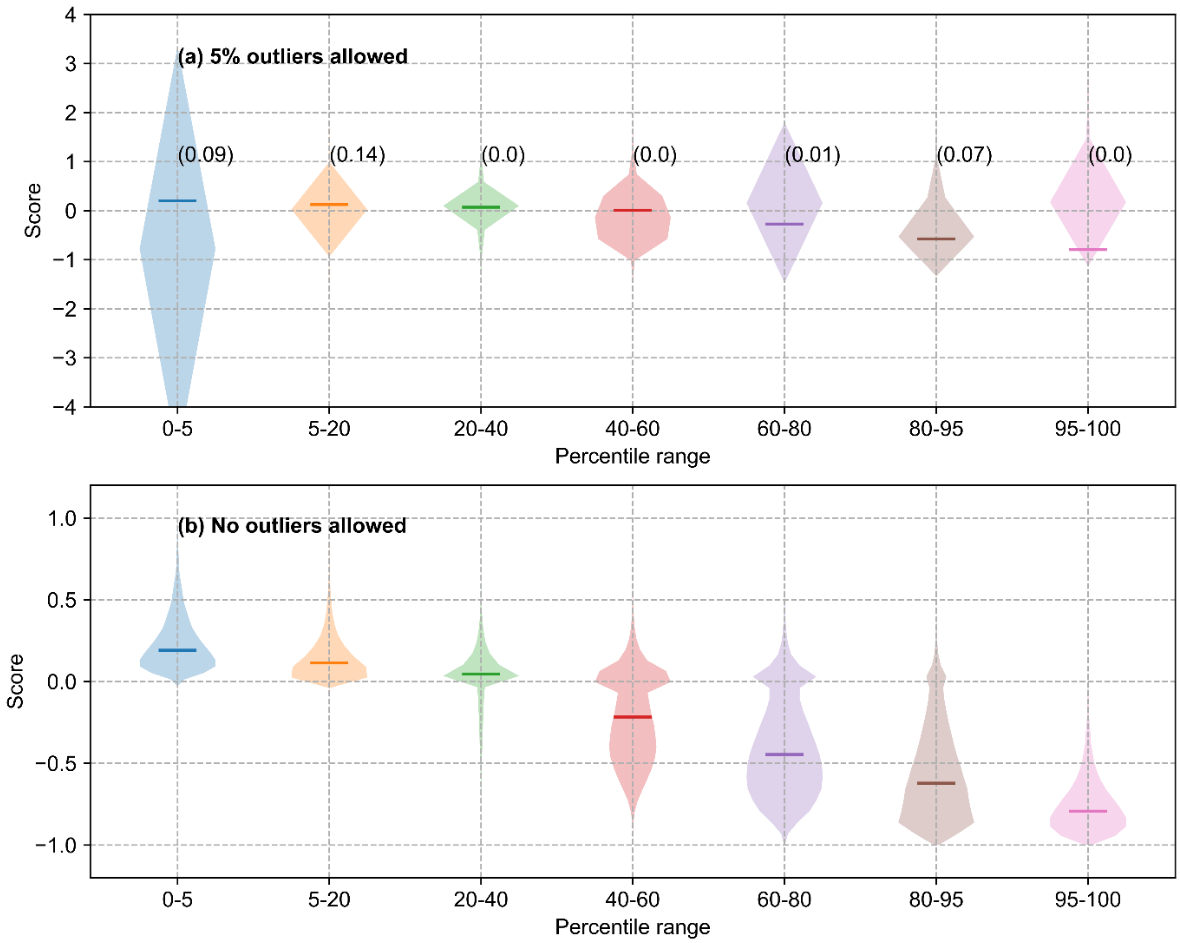

Figure S3. **Gauge 04180000, using 99.5th percentile as upper LoA, and gauged-single scenario**. The violin plots of calibration period score values for different percentile ranges. The numbers in bracket in the subplot (a) are the percentage of simulated flow values with absolute score values greater than 4.

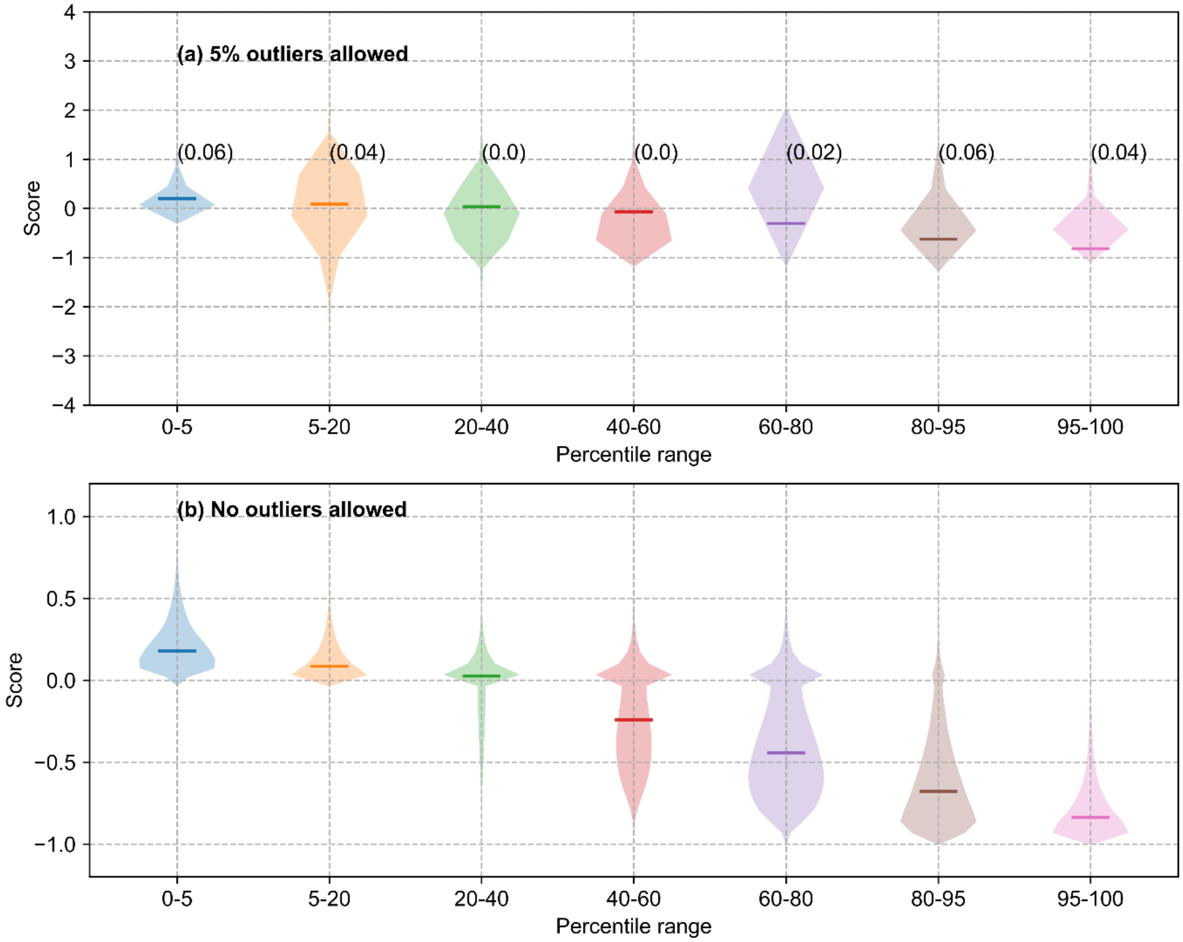

Figure S4. **Gauge 04179520, using 99.5th percentile as upper LoA, and gauged-single scenario**. The violin plots of calibration period score values for different percentile ranges. The numbers in bracket in the subplot (a) are the percentage of simulated flow values with absolute score values greater than 4.

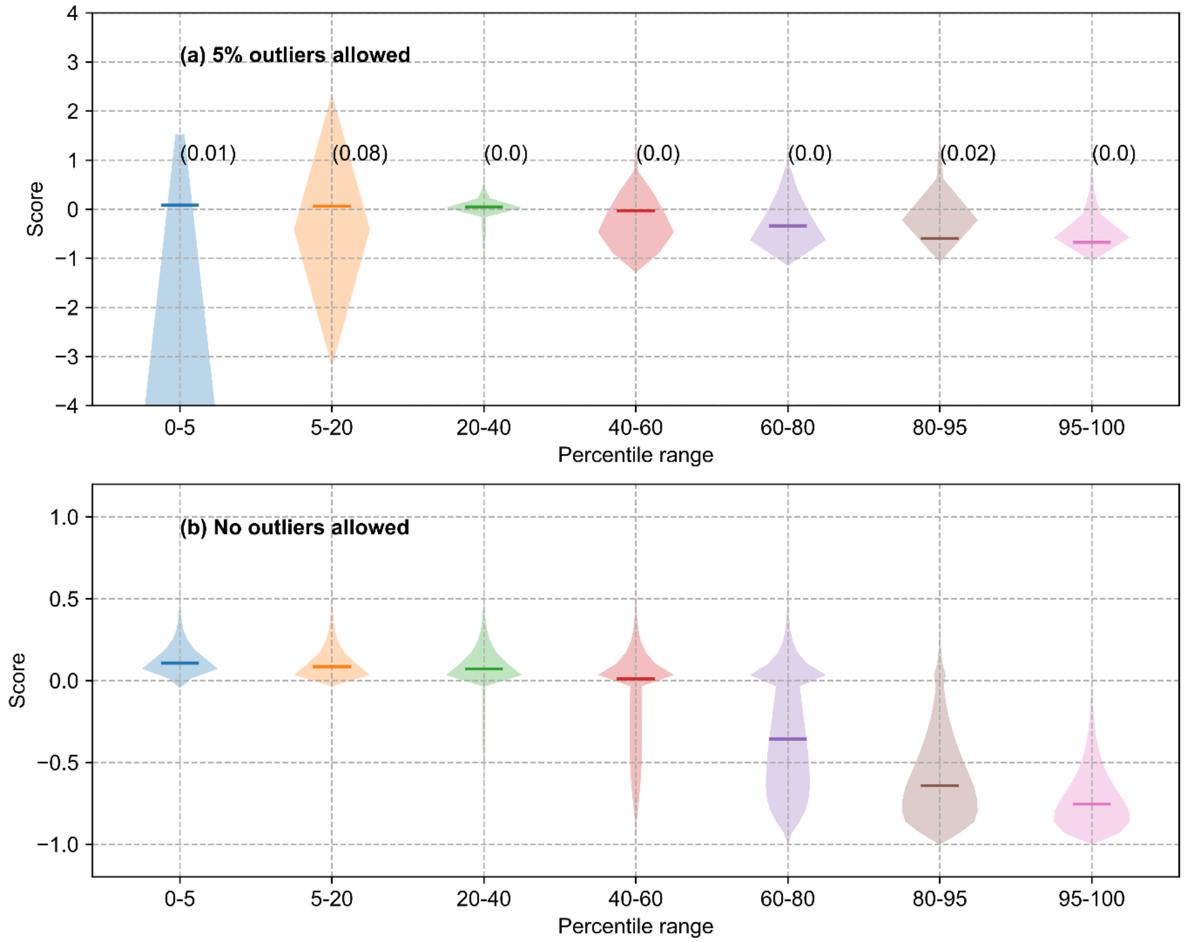

Figure S5. **Gauge 04178000, using 99.5th percentile as upper LoA, and gauged-single scenario**. The violin plots of calibration period score values for different percentile ranges. The numbers in bracket in the subplot (a) are the percentage of simulated flow values with absolute score values greater than 4.

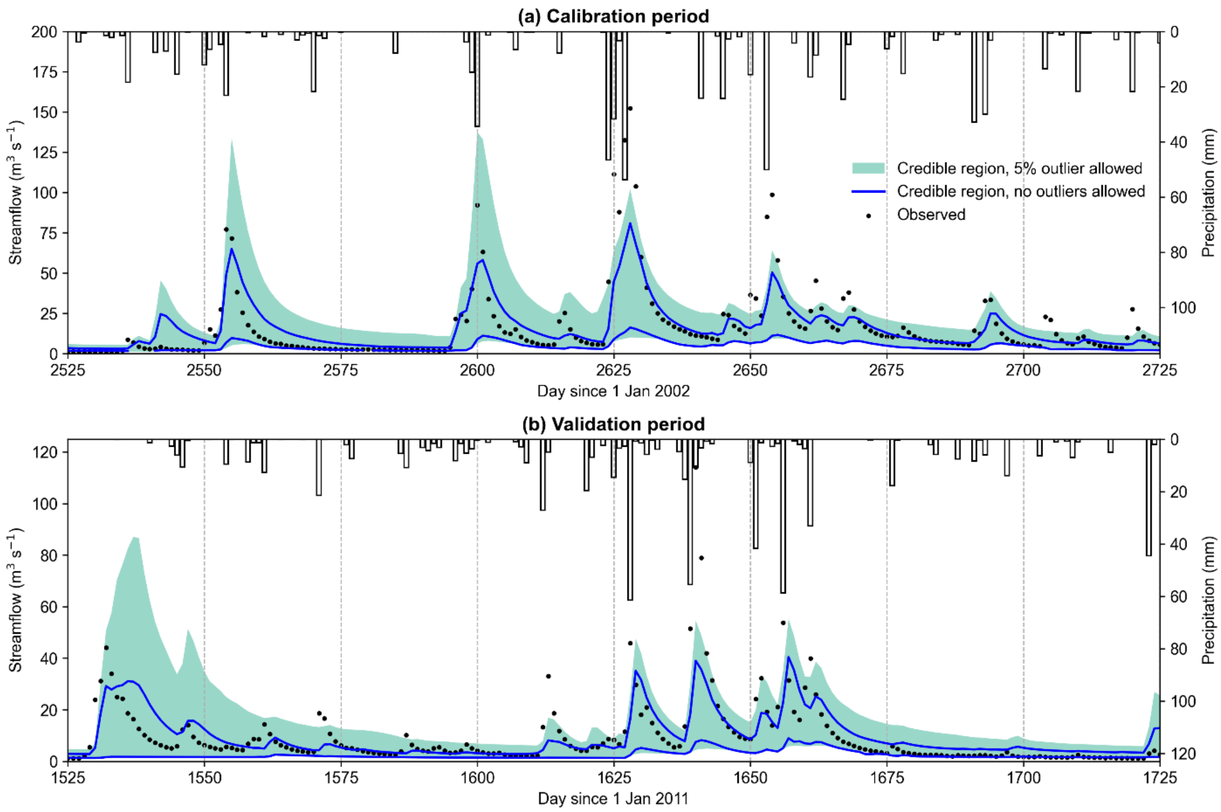

Figure S6. **Gauge 04180000, using 99.5th percentile as upper LoA, and gauged-single scenario**. Credible region of streamflow during calibration and validation periods obtained by allowing 5% outliers and no outliers.

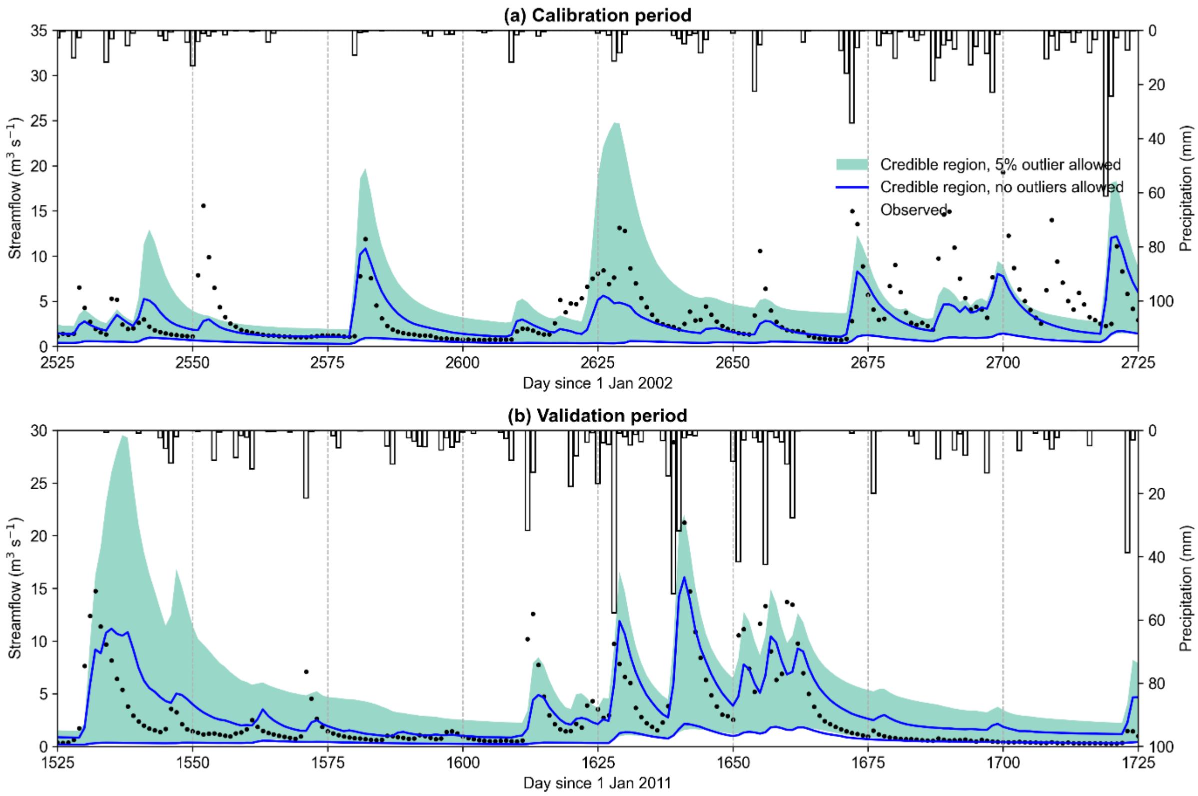

Figure S7. **Gauge 04179520, using 99.5th percentile as upper LoA, and gauged-single scenario**. Credible region of streamflow during calibration and validation periods obtained by allowing 5% outliers and no outliers.

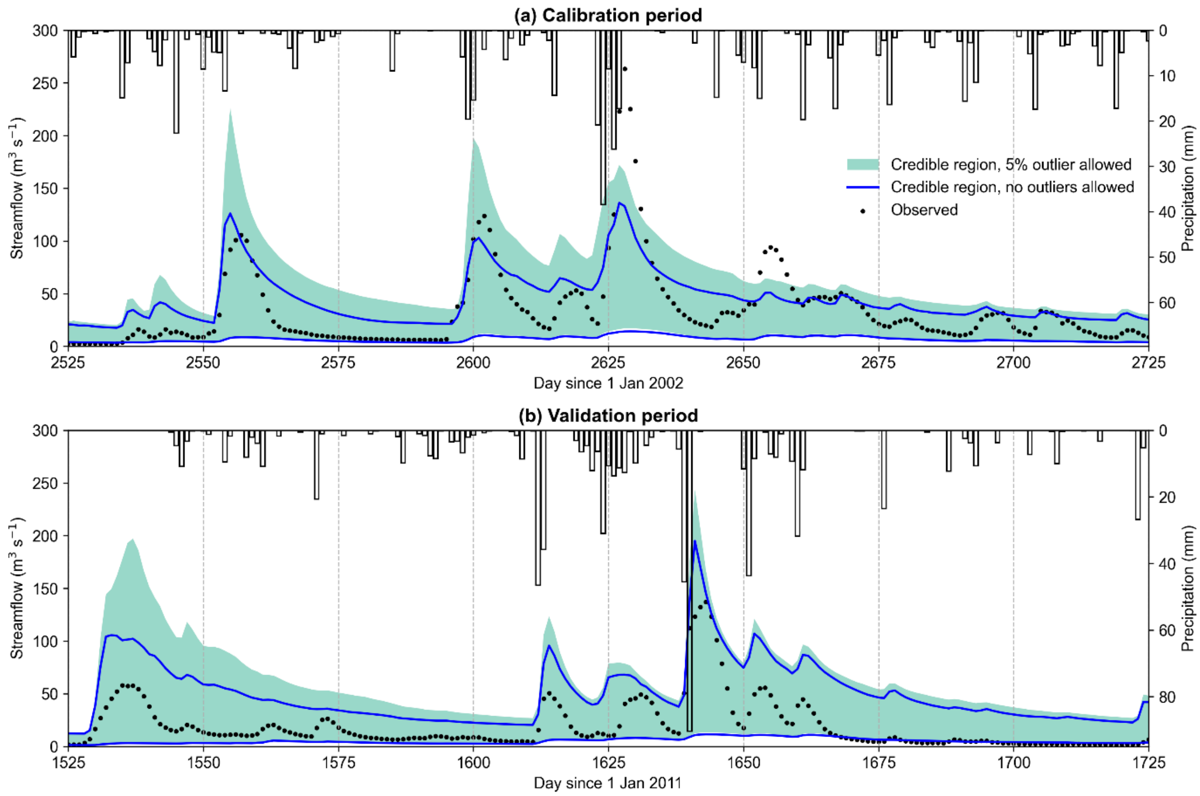

Figure S8. **Gauge 04178000, using 99.5th percentile as upper LoA, and gauged-single scenario**. Credible region of streamflow during calibration and validation periods obtained by allowing 5% outliers and no outliers.

S3. Gauged Scenario

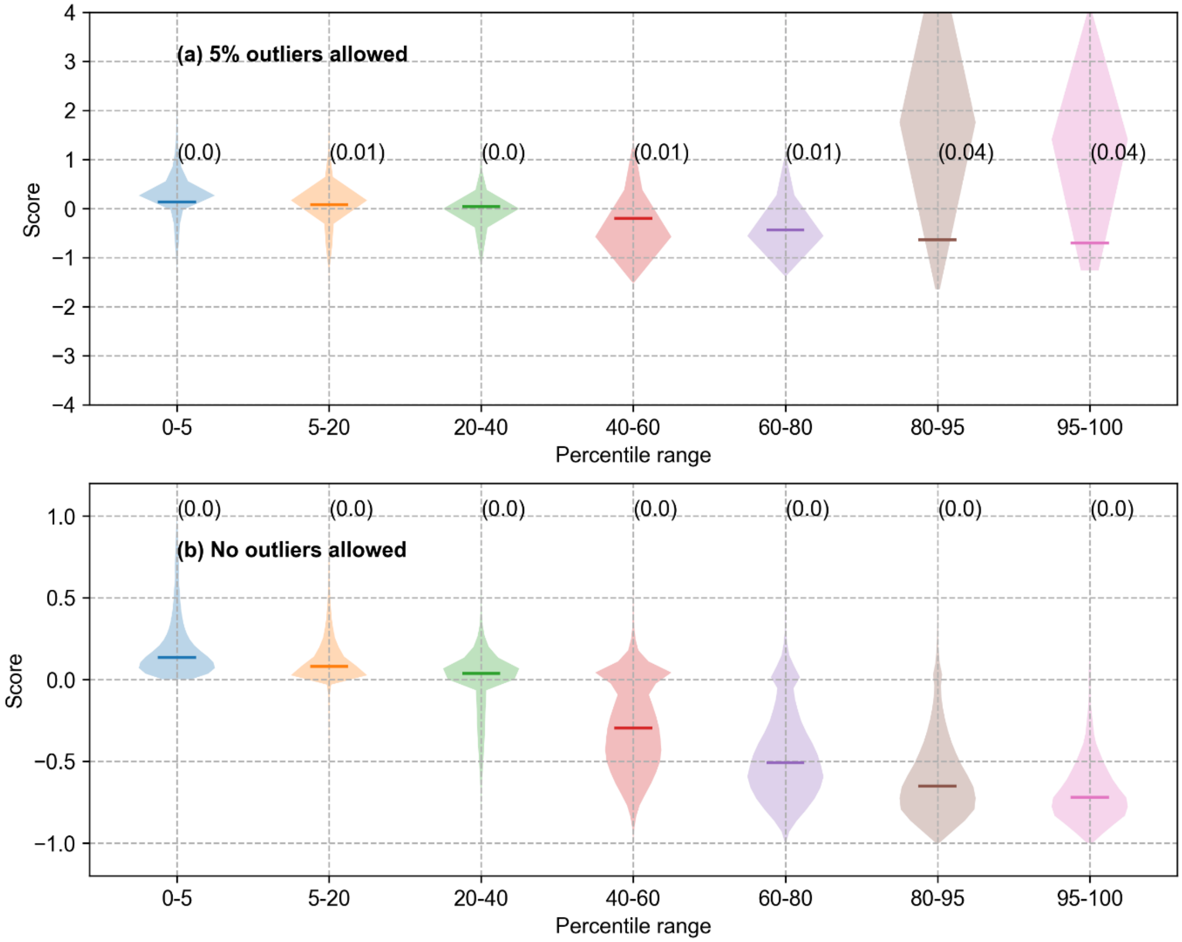

Figure S9. **Gauge 04180000, using 99.5th percentile as upper LoA, and gauged scenario**. The violin plots of calibration period score values for different percentile ranges. The numbers in bracket in the subplot (a) are the percentage of simulated flow values with absolute score values greater than 4.

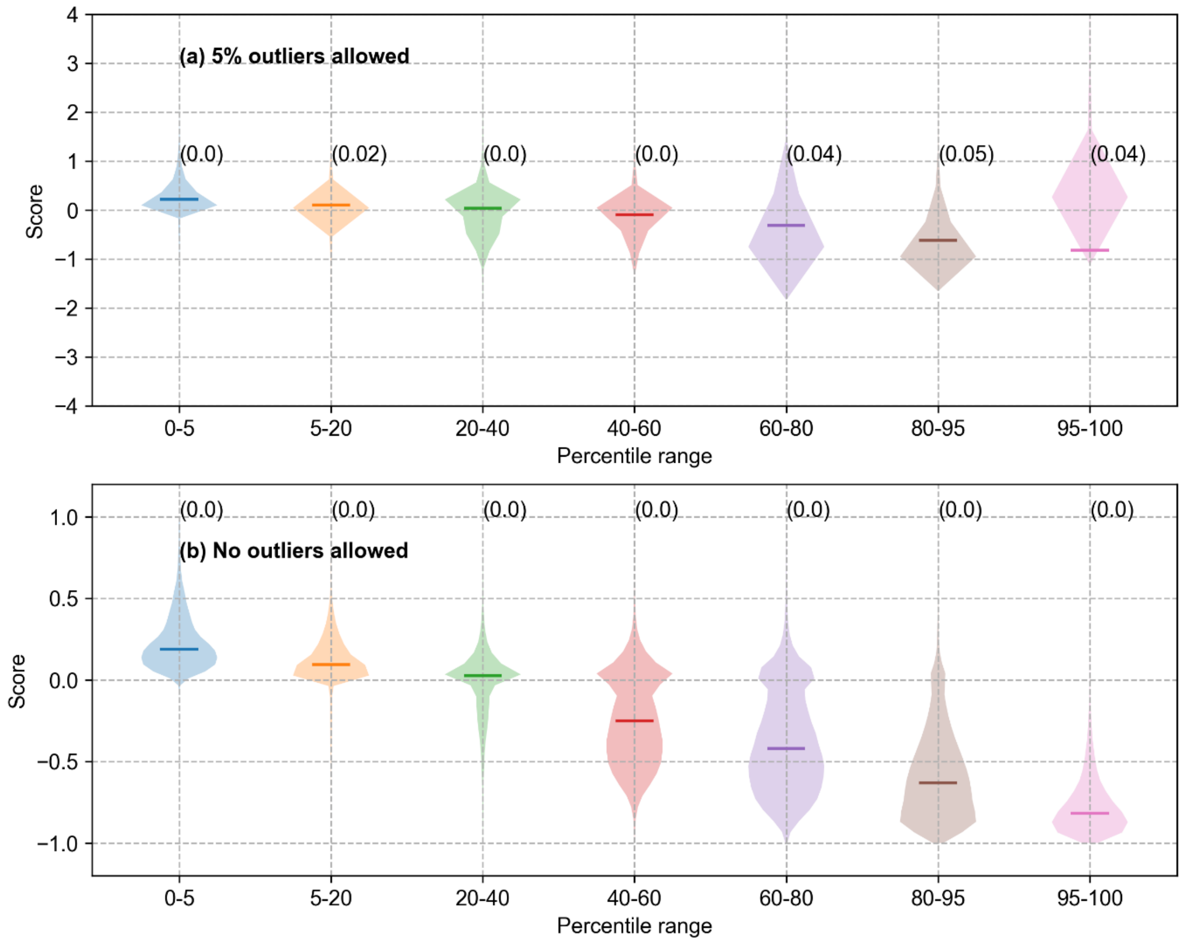

Figure S10. **Gauge 04179520, using 99.5^{th} percentile as upper LoA, and gauged scenario**. The violin plots of calibration period score values for different percentile ranges. The numbers in bracket in the subplot (a) are the percentage of simulated flow values with absolute score values greater than 4.

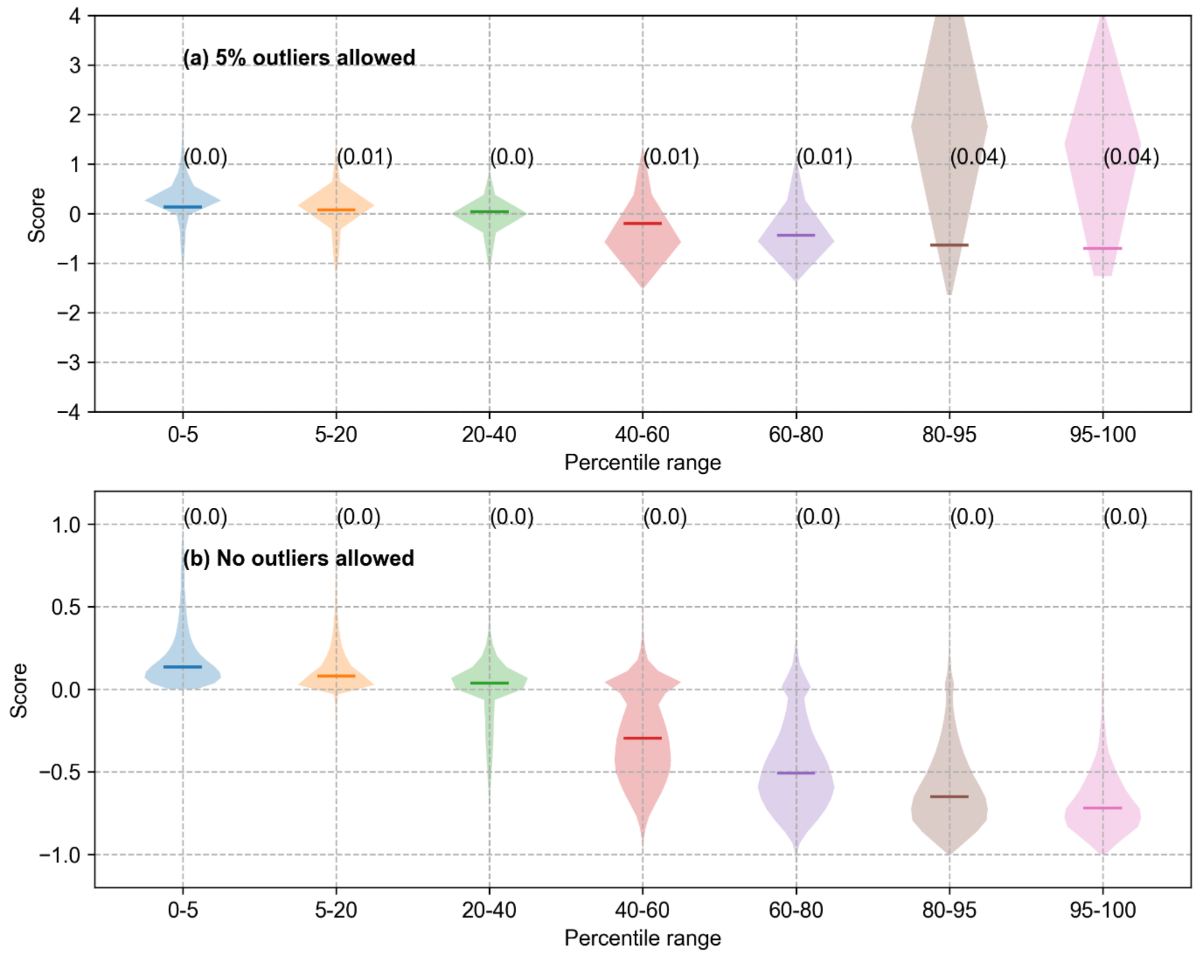

1226 Figure S11. **Gauge 04178000, using 99.5th percentile as upper LoA, and gauged scenario**.
1227 The violin plots of calibration period score values for different percentile ranges. The numbers in
1228 bracket in the subplot (a) are the percentage of simulated flow values with absolute score values
1229 greater than 4.

1230

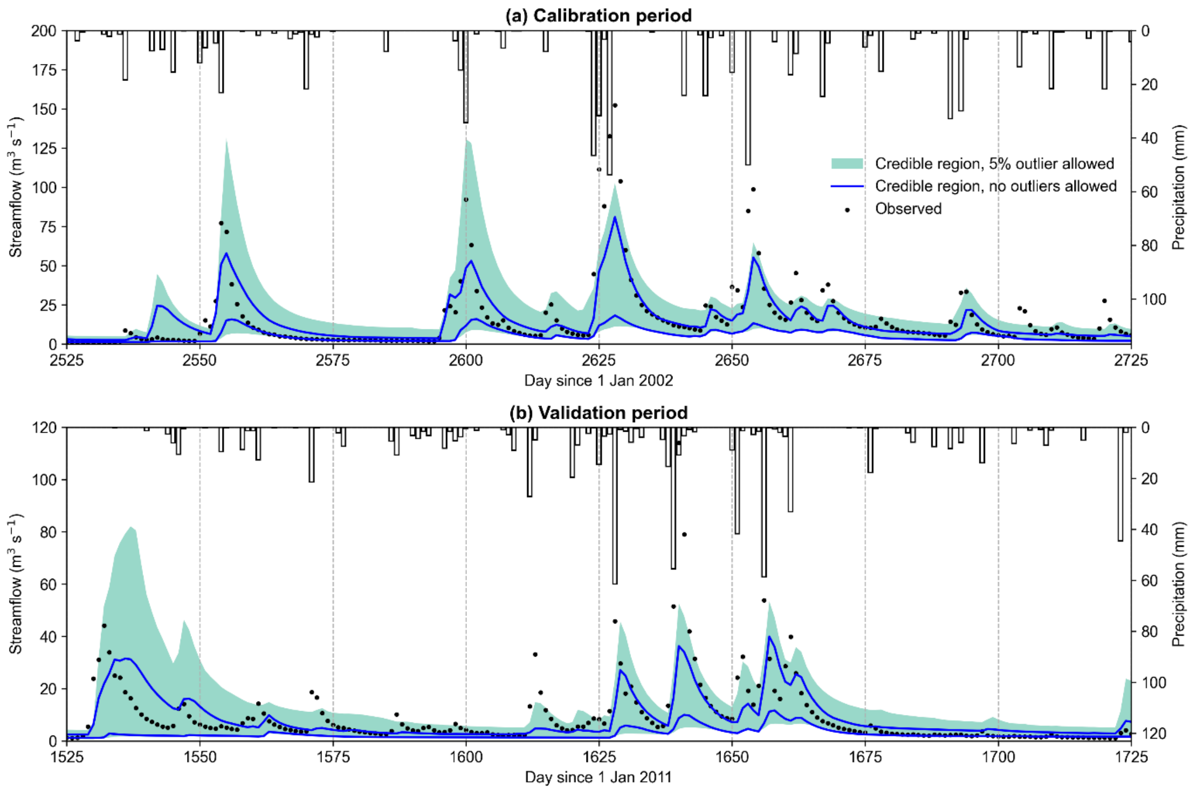

Figure S12. **Gauge 04180000, using 99.5th percentile as upper LoA, and gauged scenario**. Credible region of streamflow during calibration and validation periods obtained by allowing 5% outliers and no outliers.

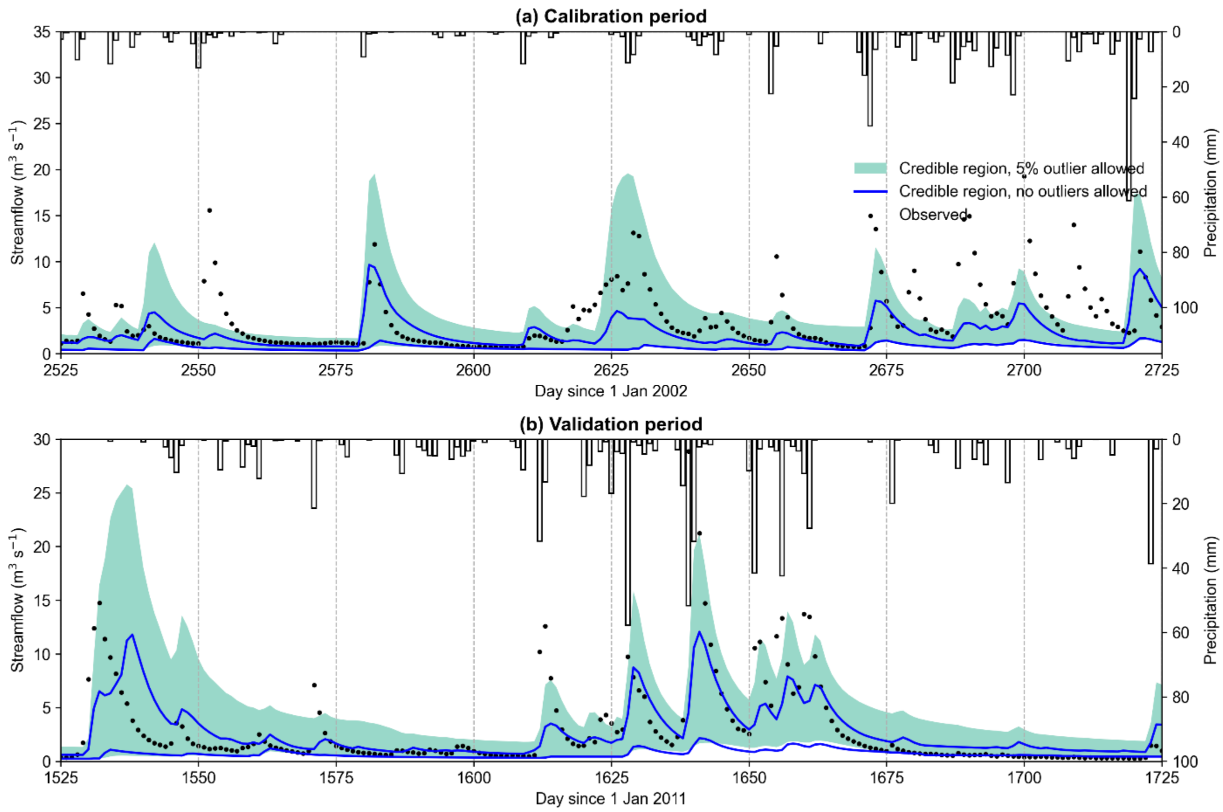

Figure S13. **Gauge 04179520, using 99.5th percentile as upper LoA, and gauged scenario**. Credible region of streamflow during calibration and validation periods obtained by allowing 5% outliers and no outliers.

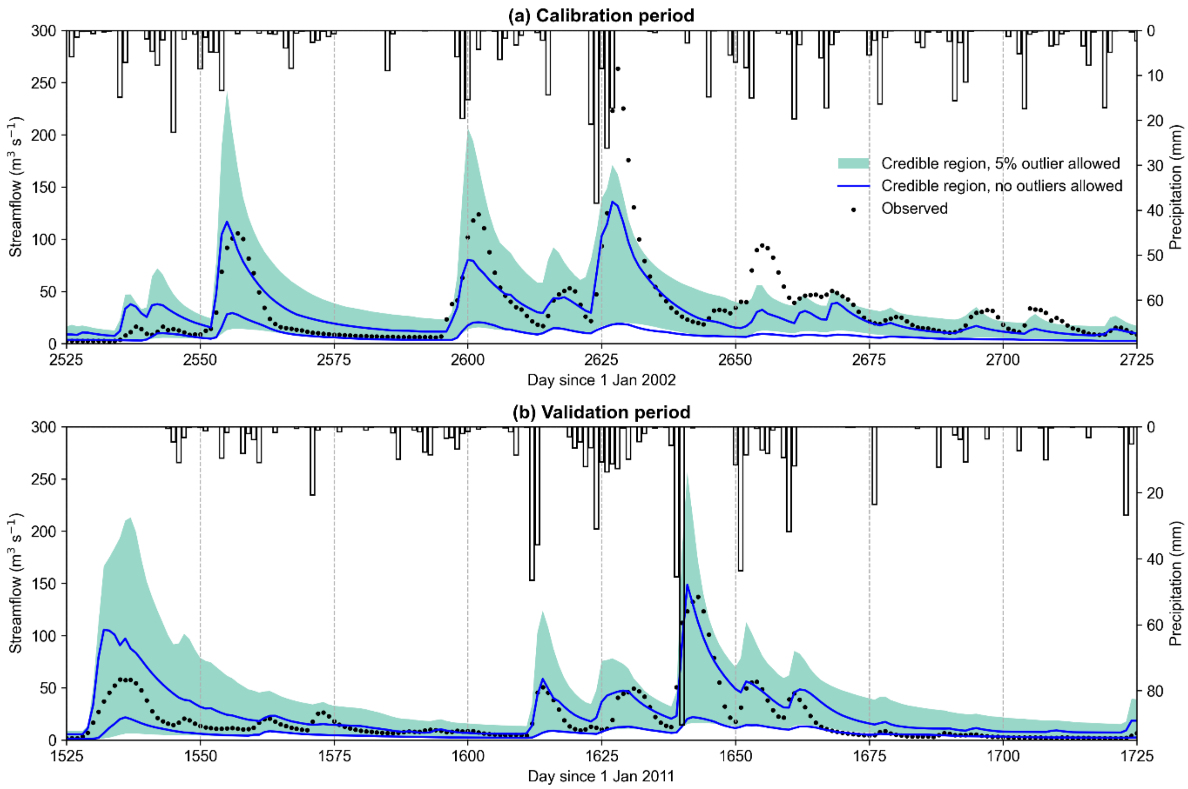

Figure S14. **Gauge 04178000, using 99.5th percentile as upper LoA, and gauged scenario**. Credible region of streamflow during calibration and validation periods obtained by allowing 5% outliers and no outliers.

S4. Effect of streamflow signature constraints on constraining the simulations in gauged scenarios

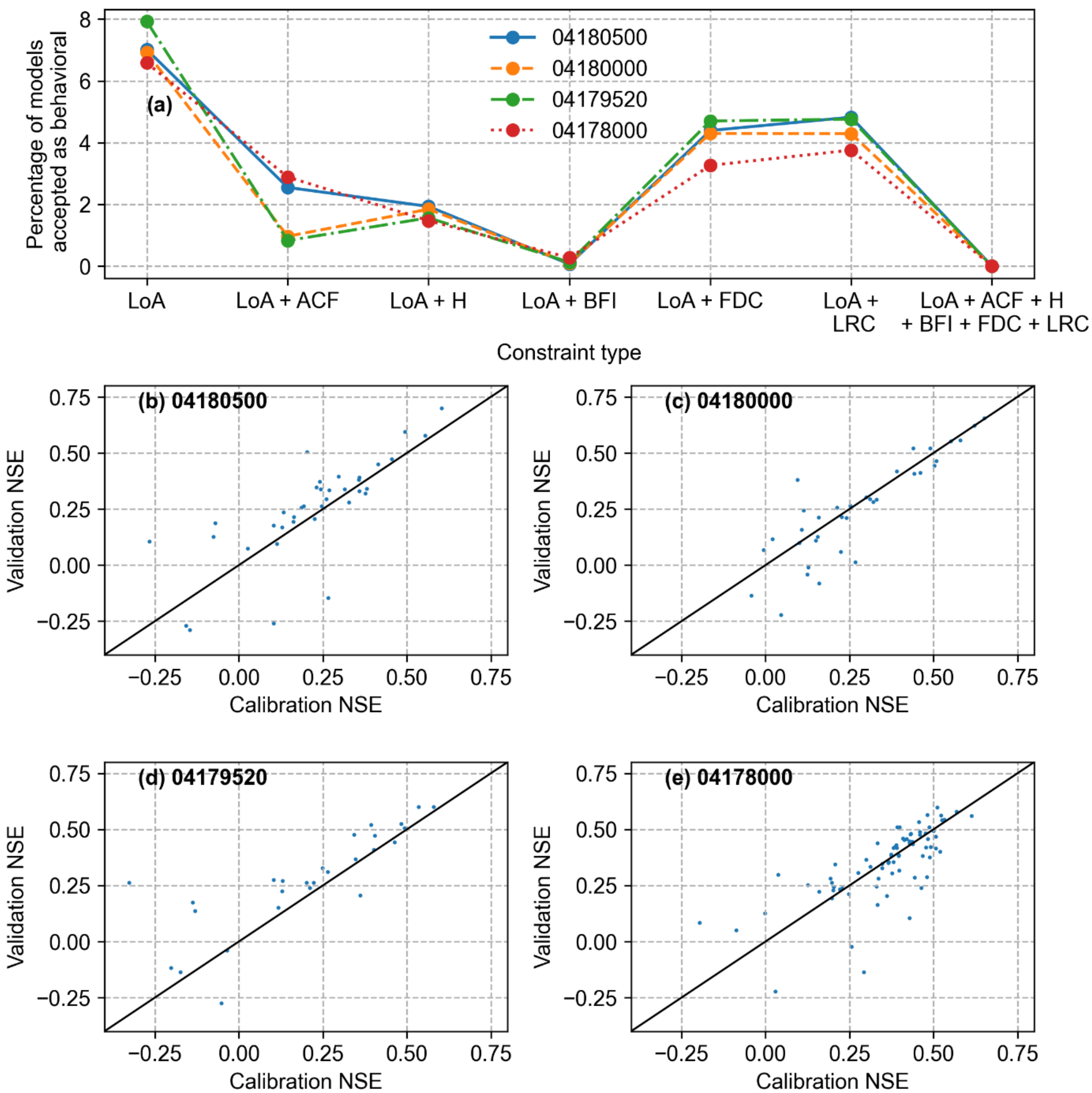

Figure S15. **Gauged scenario. (a)** Percentage of models accepted as behavioral, obtained by applying different constraints; **(b), (c), (d)** and **(e)** calibration and validation NSEs for the behavioral obtained by applying all the constrains.

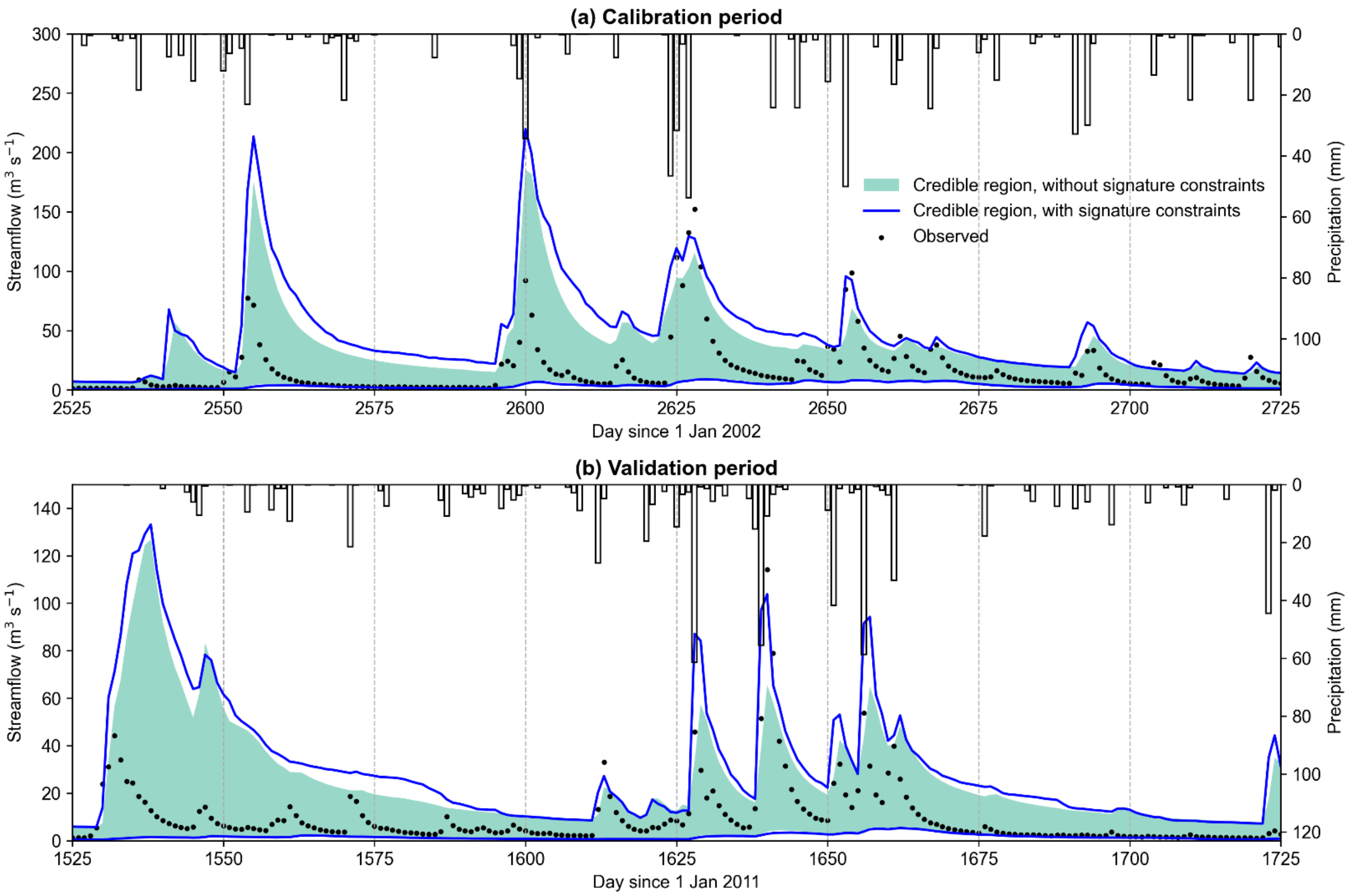

Figure S16. **Gauge 04180000, using 99.5th percentile as upper LoA, and gauged-single scenario**. Credible region of streamflow during calibration and validation periods obtained by allowing 5% outliers when the model was constrained only using LoAs (green band) and when the model was constrained using LoA and other constraints (blue band).

1251

1252

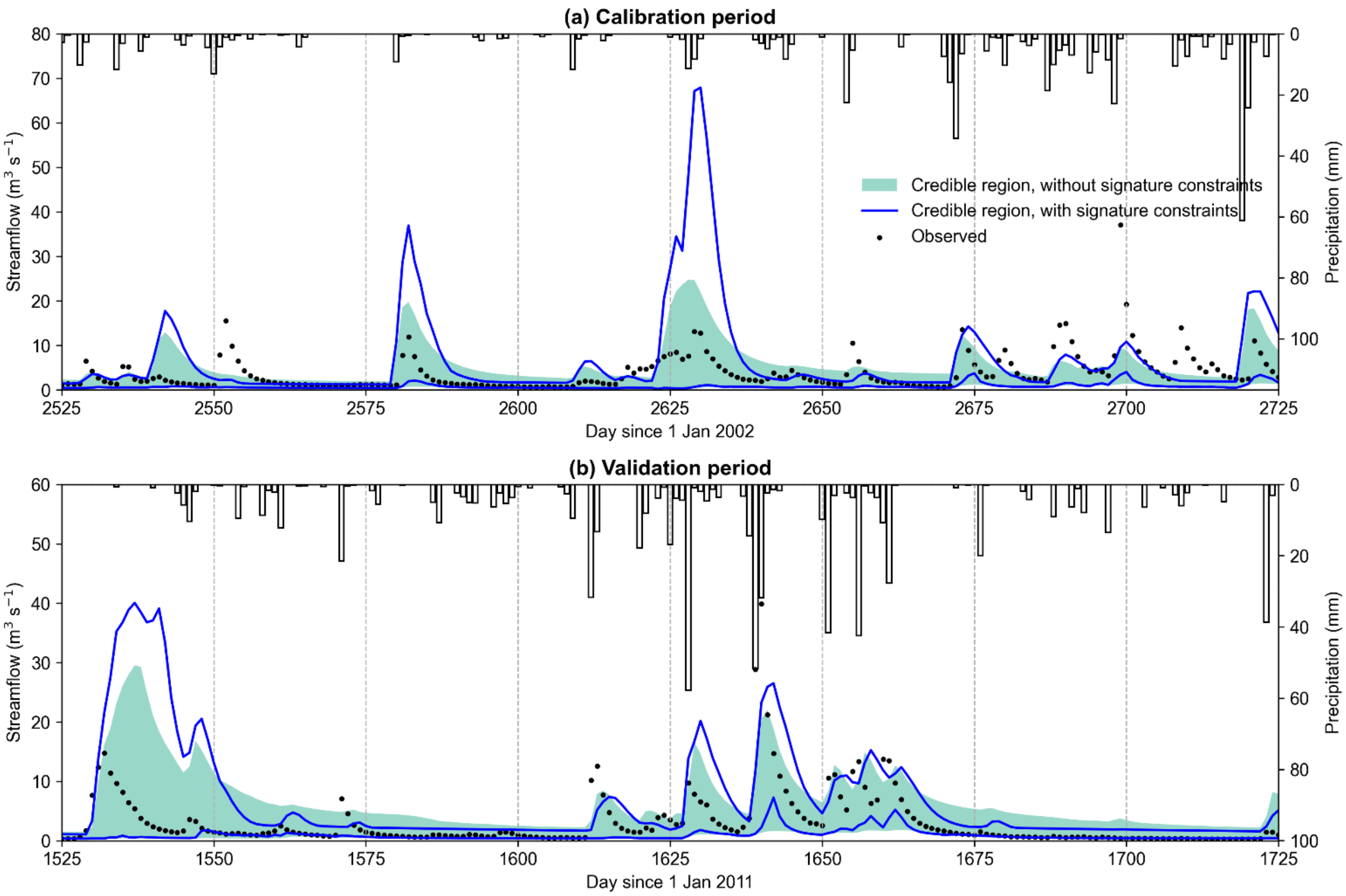

Figure S17. **Gauge 04179520, using 99.5th percentile as upper LoA, and gauged-single scenario**. Credible region of streamflow during calibration and validation periods obtained by allowing 5% outliers when the model was constrained only using LoAs (green band) and when the model was constrained using LoA and other constraints (blue band).

1253

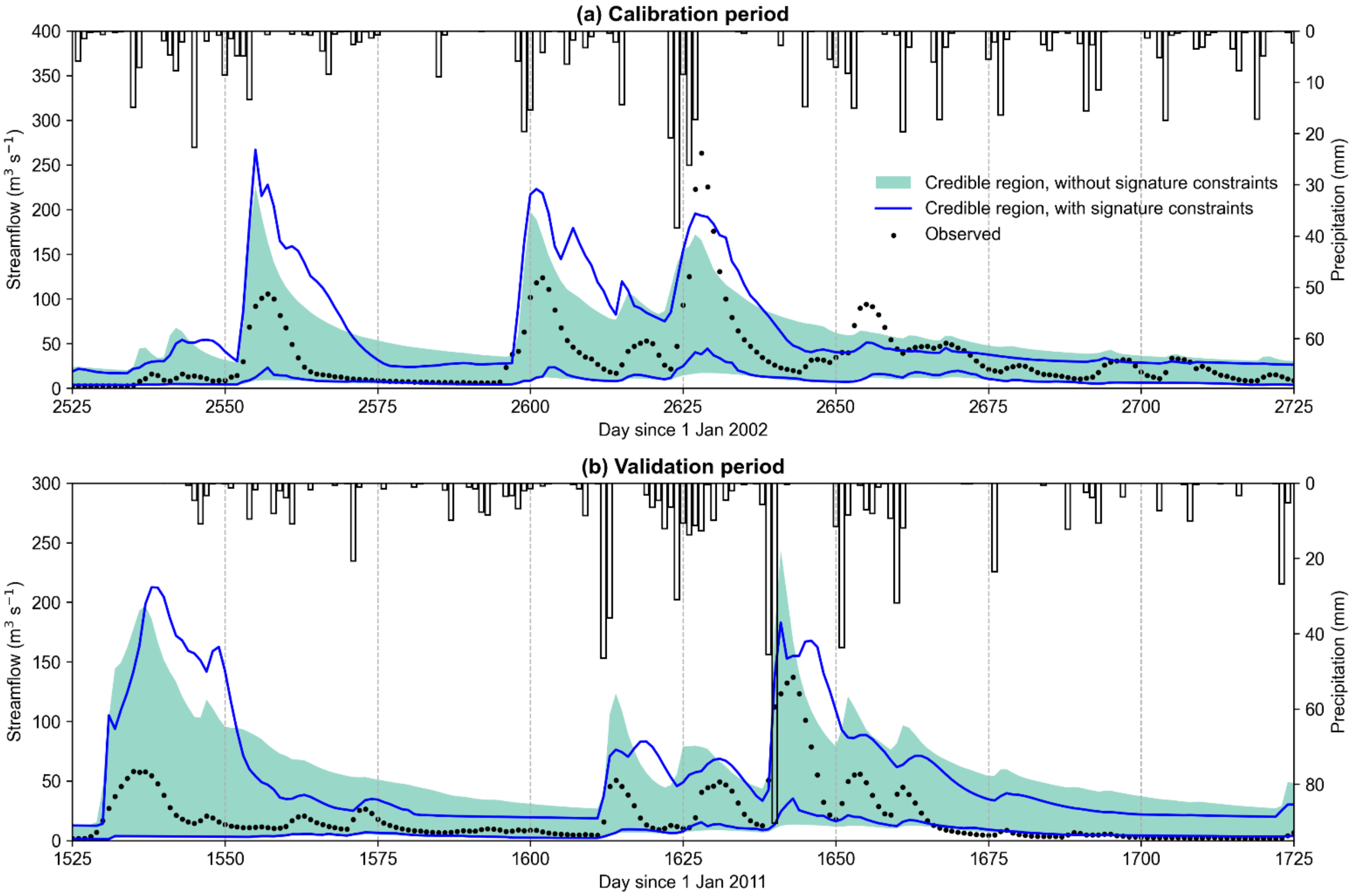

Figure S18. **Gauge 04178000, using 99.5th percentile as upper LoA, and gauged-single scenario**. Credible region of streamflow during calibration and validation periods obtained by allowing 5% outliers when the model was constrained only using LoAs (green band) and when the model was constrained using LoA and other constraints (blue band).

S5. Analysis of the ungauged scenario

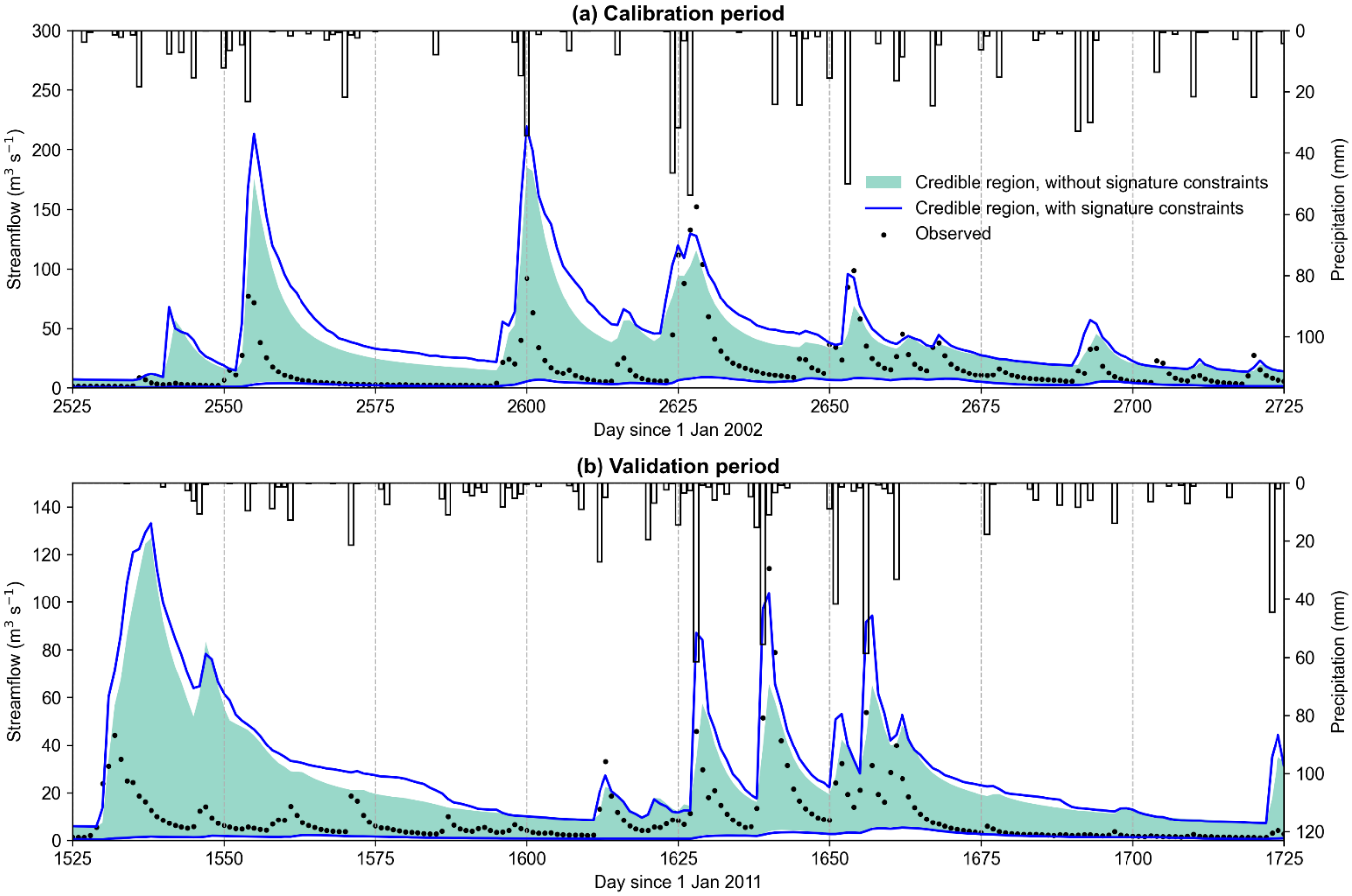

Figure S19. **Gauge 04180000, using 99.5th percentile as upper LoA, and ungauged scenario**. Credible region of streamflow during calibration and validation periods obtained by allowing 5% outliers when the model was constrained only using LoAs (green band) and when the model was constrained using LoA and other constraints (blue band).

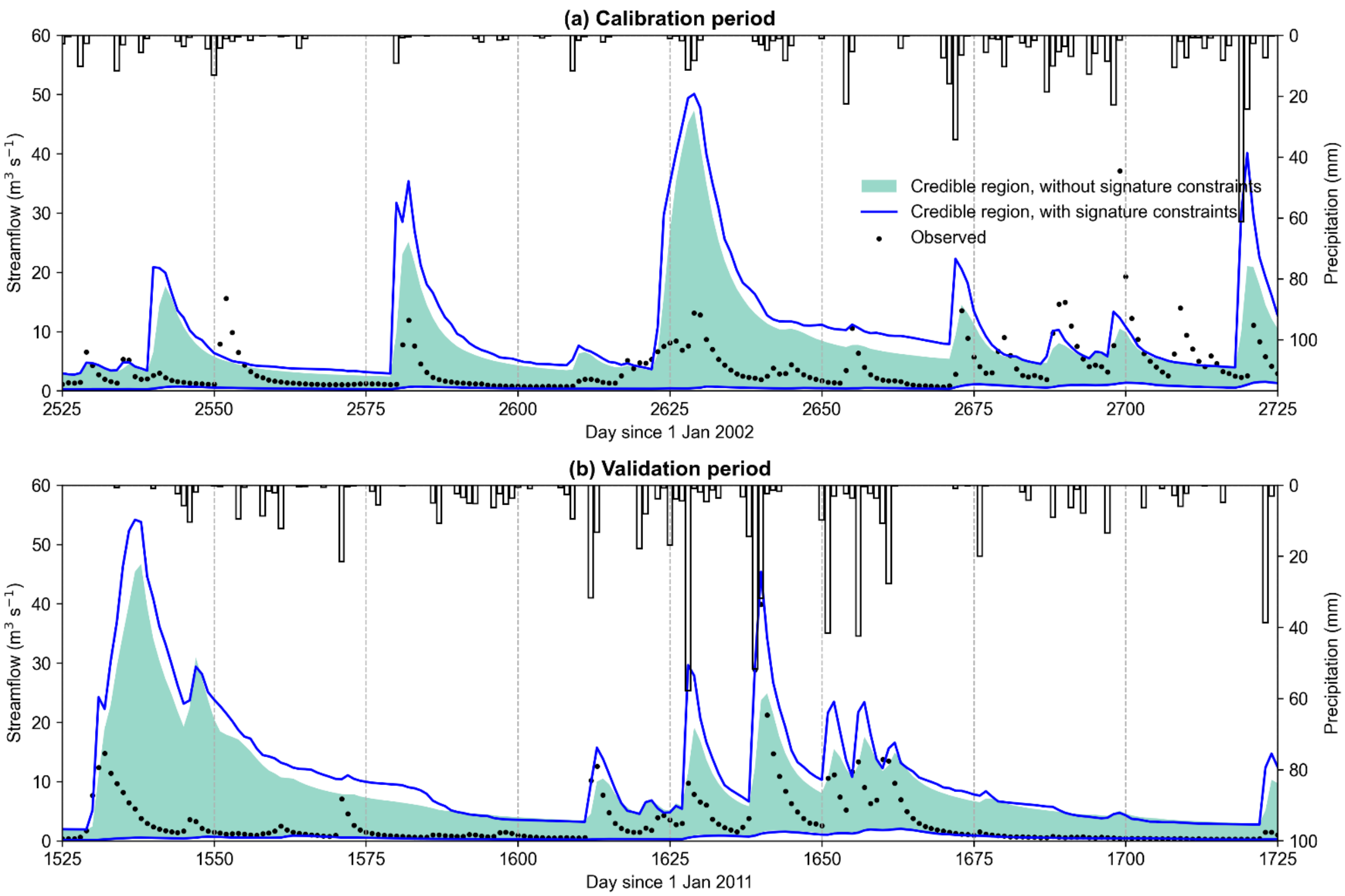

Figure S20. **Gauge 04179520, using 99.5^{th} percentile as upper LoA, and ungauged scenario**. Credible region of streamflow during calibration and validation periods obtained by allowing 5% outliers when the model was constrained only using LoAs (green band) and when the model was constrained using LoA and other constraints (blue band).

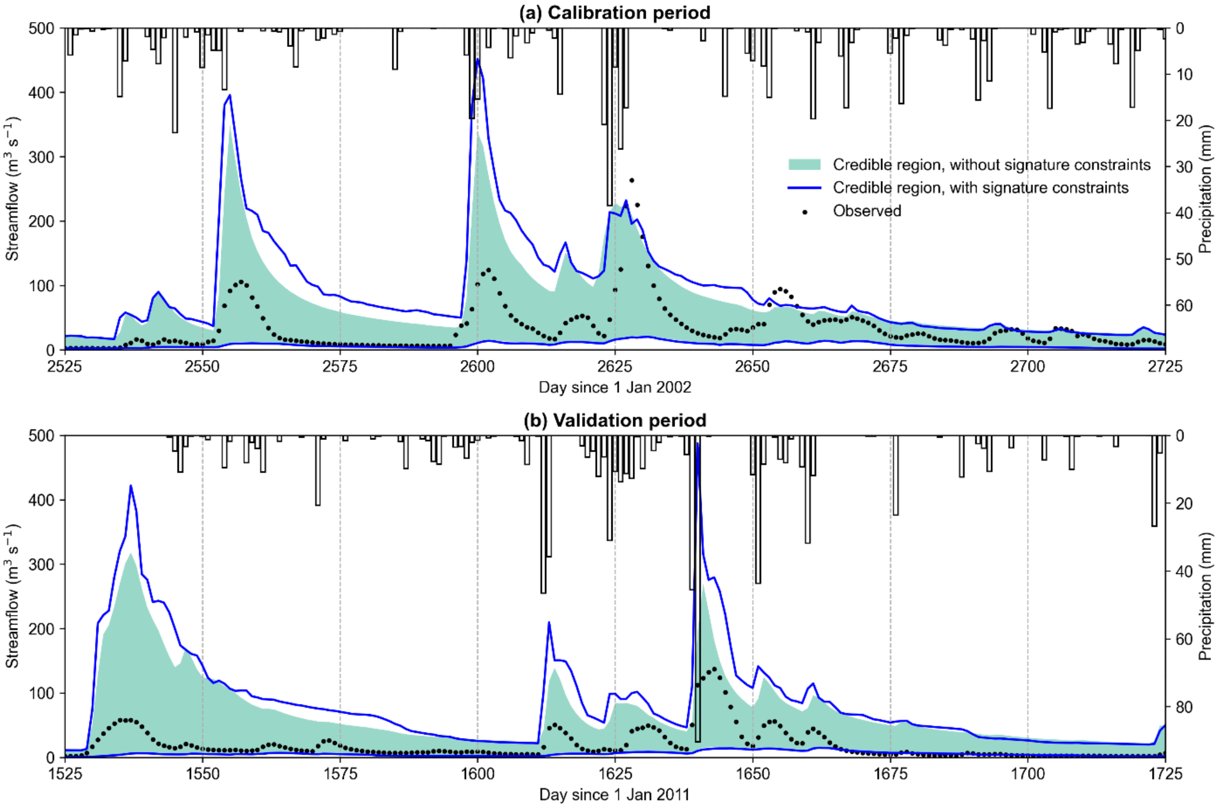

Figure S21. **Gauge 04178000, using 99.5th percentile as upper LoA, and ungauged scenario**. Credible region of streamflow during calibration and validation periods obtained by allowing 5% outliers when the model was constrained only using LoAs (green band) and when the model was constrained using LoA and other constraints (blue band).